Meson-Exchange Currents in Quasielastic Electron Scattering in a Generalized Superscaling Approach

Paloma Rodriguez Casale , Jose Enrique Amaro * , Maria B. Barbaro

Posted Date: 1 August 2023

doi: 10.20944/preprints202308.0066.v1

Keywords: superscaling; quasielastic electron scattering; meson-exchange currents, relativistic mean field

Article

Meson-Exchange Currents in Quasielastic Electron Scattering in a Generalized Superscaling Approach

Paloma Rodriguez Casale [1,2], Jose E Amaro [1,2,*] and Maria B. Barbaro [3,4]

[1] Departamento de Física Atómica, Molecular y Nuclear, 18071 Granada, Spain
[2] Instituto Carlos I de Física Teórica y Computacional, Universidad de Granada, 18071 Granada, Spain
[3] Dipartimento di Fisica, Università di Torino, 10125 Torino, Italy
[4] INFN Sezione di Torino, 10125 Torino, Italy
* Correspondence: amaro@ugr.es

Abstract: We present a model that incorporates the effect of two-body currents in quasielastic electron-nucleus scattering within the framework of a consistent superscaling formalism. This is achieved by defining an averaged single-nucleon hadronic tensor based on the 1p1h matrix element of the one-body current plus meson-exchange currents (MEC). The consistent treatment of one- and two-body currents in our model enables the calculation of exchange current effects in the kinematical region where the Fermi gas response is zero, but not the scaling function. The effect of MEC is consistently taken into account when extracting the phenomenological scaling function from electron scattering data. With this model, we investigate the effect of MEC on the response functions taking into account the effective mass of the nucleon, and examine the consequences it has on the inclusive (e, e') cross section. We find that 1p1h MEC deplete the quasielastic transverse response, while they not alter significantly the scaling behavior of (e, e') data.

Keywords: superscaling; quasielastic electron scattering; meson-exchange currents; relativistic mean field

1. Introduction

The pursuit of neutrino oscillation experiments represents a significant scientific endeavor, encompassing both experimental and theoretical efforts [1–6]. In particular, theoretical nuclear physics has been propelled to analyze neutrino-induced nuclear reactions in these experiments [7–16]. The ultimate goal is to minimize uncertainties arising from nuclear effects, which are a primary source of systematic errors when determining the neutrino interactions in detectors. Simultaneously, there has been a renewed interest in electron scattering studies [17–21], as theoretical models can be calibrated using (e,e′) data and subsequently extended to neutrinos by incorporating the contribution of the axial current.

At typical energies around 1 GeV in many neutrino experiments, a significant contribution arises from quasielastic nucleon emission, which dominates at transferred energies around $\omega = |Q^2|/2m_N^*$, where ω is the energy transfer, $Q^2 = \omega^2 - q^2 < 0$, and q is the momentum transfer to a nucleon with relativistic effective mass m_N^* [22–26]. It is crucial to take into account that the transferred energies involved in neutrino experiments necessitate a relativistic treatment of the reaction. This requirement introduces significant challenges in constructing appropriate models for these interactions [27–31].

In this article, we focus on the study of one-particle one hole (1p1h) transverse and longitudinal responses in the QE peak [32–34], at intermediate and high momentum transfer, including the effect of meson exchange currents (MEC) for electron scattering. The MEC are two-body currents that involve the exchange of mesons between nucleons and virtual excitation of nuclear resonances. This can have a significant impact on the scattering cross section and on the distribution of energy and momentum transferred during the interaction. The emission of two particles (2p2h), stemming from MEC and short-range correlations, has emerged as a focal point in studies on lepton-nucleus scattering.

Extensive research has been dedicated to understanding its effects on the cross-section of both electron and neutrino interactions [35–45]. However, it is often overlooked that MEC also contribute

 doi:10.20944/preprints202308.0066.v1

to the emission of a single particle (1p1h), thereby introducing interference effects with the one-body current. Notably, calculations have shown a reduction in the quasielastic transverse response compared to the impulse approximation when employing nuclear shell or Fermi gas models [17,33,41,46–49]. This reduction is mainly due to the exchange part of the 1p1h matrix element of the Δ current.

In this work, we aim also to incorporate the effect of Meson Exchange Currents (MEC) consistently into the quasielastic peak within the framework of the relativistic effective mass Superscaling (SuSAM*) model [50,51]. This is an extension of SuSA model based on the approximation of factorizing the nuclear response into a single nucleon response multiplied by a superscaling function [52]. The phenomenological superscaling function accounts for nuclear structure and reaction effects, as it is fitted to experimental data. The motivation behind scaling models arises from the observation that inclusive data, when divided by an appropriate single nucleon prefactor, approximately scale when plotted against a suitable scaling variable, ψ, extracted from the Relativistic Fermi Gas (RFG) model [52]. The SuSA model [13], along with its improved version SuSAv2, and SuSAM*, has been extensively utilized to analyze inclusive electron and neutrino scattering data [15,18,53–55]. These efforts represent important strides in understanding and predicting neutrino-nucleus interactions. By establishing a phenomenological scaling function that successfully describes (e,e') data, these models provide a valuable foundation for extrapolating to neutrino cross-sections.

The SuSAM* model builds upon the SuSA framework but incorporates the effective mass dependence from the Relativistic Mean Field (RMF) theory. A notable feature of the RMF model of nuclear matter (such as the Walecka or $\sigma - \omega$ model [23]) is that it reproduces the (e,e') cross-section better than the RFG model when an appropriate value for the effective mass M* is chosen [22,25,56]. Motivated by this the SuSAM* model employs the RMF model's scaling variable, ψ^*, and single nucleon prefactor dependent on the effective mass, with the aim to capture the essential dynamics associated with the interaction process more accurately. This approach capitalizes on the reasonable dynamical aspects embedded in the RMF model and offers an alternative description of the scaling behavior observed electron scattering cross section. It provides a comprehensive framework that combines the strengths of the RMF model and the superscaling formalism, leading to an improved understanding and interpretation of experimental data.

Until now, a unified model that incorporates 1p1h Meson Exchange Currents in the superscaling function had not been proposed. This was primarily due to the violation of scaling properties by MEC, even at the Fermi gas level [32]. Additionally, the 1p1h matrix element of MEC is not easily extrapolated to the $|\psi| > 1$ region outside the range where the Fermi gas response is zero, as nucleons are constrained by the Fermi momentum. In this work, we address both of these challenges in a unified manner by modifying the scaling model to account for the contribution of MEC within the single nucleon prefactor. Furthermore, we take the opportunity to enhance the recently improved superscaling model by eliminating the extrapolation of single-nucleon responses averaged over the Fermi gas to the region $|\psi| > 1$ [57]. Instead of extrapolation, we introduce a new approach where the single nucleon response is averaged with a smeared momentum distribution around the Fermi surface. As a result, the averaged single nucleon responses are well defined for all the values of ψ.

In the modified superscaling framework proposed in this work, the single nucleon response incorporates the contribution of MEC to the effective one-body current operator. This modification allows us to define a new prefactor that already includes the effects of MEC, enabling a novel scaling analysis of the data. Importantly, it should be noted that the Fermi gas now exhibits exact scaling behavior when utilizing the new single nucleon response: scaling violations associated to the MEC are exactly canceled by the dividing factor used to construct the scaling function. By incorporating these modifications, we overcome the limitations of previous models and provide a comprehensive framework that encompasses both MEC and modified superscaling effects. By consistently integrating 1p1h MEC within the SuSAM* model, we aim at refining our understanding of the underlying nuclear dynamics in the quasielastic peak. This comprehensive approach allows us to account for both the

Preprints (www.preprints.org) | NOT PEER-REVIEWED | Posted: 1 August 2023 doi:10.20944/preprints202308.0066.v1

scaling behavior observed in inclusive data and the contributions from meson exchange currents, leading to a more accurate and comprehensive description of the reaction.

The article is structured as follows. In Sect. 2, we introduce the formalism of quasielastic electron scattering within the framework of the Relativistic Mean Field (RMF) model of nuclear matter, incorporating Meson Exchange Currents (MEC). In Sect. 3, we present our unified scaling model that incorporates MEC effects. We describe the modifications made to the conventional scaling approach to account for the contribution of MEC within the single nucleon prefactor. In Sect. 4 we present the results of our calculations and analyses based on the unified scaling model with MEC. Finally in Sect. 5 we present the conclusions drawn from our study.

2. Formalism

2.1. Response functions

We start with the inclusive electron scattering cross section in plane-wave Born approximation with one photon-exchange. The exchanged photon transfers an energy ω and a momentum $\mathbf{q}$ to the nucleus. The initial electron energy is ϵ, the scattering angle is θ, and the final electron energy is $\epsilon' = \epsilon - \omega$. The double-differential cross section is written in terms of the longitudinal and transverse response functions, $R_L(q,\omega)$ and $R_T(q,\omega)$,

$$\frac{d\sigma}{d\Omega d\epsilon'} = \sigma_{\text{Mott}} \left(v_L R_L(q,\omega) + v_T R_T(q,\omega) \right), \tag{1}$$

where σ_{Mott} is the Mott cross section and v_L and v_T are the kinematic coefficients defined as

$$v_L = \frac{Q^4}{q^4} \tag{2}$$

$$v_T = \tan \frac{Q^4}{q^4} - \frac{Q^2}{2q^2} \tag{3}$$

with $Q^2 = \omega^2 - q^2 < 0$ the four-momentum transfer. The nuclear response functions are the following combinations of the hadronic tensor

$$R_L = W^{00}, \qquad R_T = W^{11} + W^{22}. \tag{4}$$

The inclusive hadronic tensor is constructed from the matrix elements of the electromagnetic current operator $\hat{J}^\mu(\mathbf{q})$ between the initial and final hadronic states:

$$\begin{aligned} W^{\mu\nu} &= \sum_f \overline{\sum_i} \langle f | \hat{J}^\mu(\mathbf{q}) | i \rangle^* \langle f | \hat{J}^\nu(\mathbf{q}) | i \rangle \\ &\times \delta(E_f - E_i - \omega), \end{aligned} \tag{5}$$

where the sum is performed over the undetected final nuclear states $|f\rangle$ and the average over the initial ground state $|i\rangle$ spin components.

In this work, our approach aims at exploting the scaling symmetry of quasielastic data. This scaling symmetry states that the scaling function, that is, the cross-section divided by an appropriately averaged single-nucleon cross-section and multiplied by a kinematic factor, only depends on a single kinematic variable, ψ, rather than on the three variables (ϵ, q, ω). The scaling function is approximately the same for all nuclei [51]. The starting point for the scaling analysis is the relativistic Fermi gas (RFG) model, where this symmetry holds exactly. In the case of real nuclei, it is only approximately fulfilled, but it proves to be very useful for analyzing experimental data and performing calculations and predictions.

Preprints (www.preprints.org) | NOT PEER-REVIEWED | Posted: 1 August 2023 doi:10.20944/preprints202308.0066.v1

2.2. 1p1h hadronic tensor

In independent particle models, the main contribution to the hadronic tensor in the quasielastic peak comes from the one-particle one-hole (1p1h) final states. As the transferred energy increases, there are contributions from two-particle two-hole (2p2h) emission, the inelastic contribution of pion emission above the pion mass threshold, and the deep inelastic scattering at higher energies. Therefore, the hadronic tensor can be generally decomposed as the sum of the 1p1h contribution and other contributions:

$$W^{\mu\nu} = W^{\mu\nu}_{1p1h} + W^{\mu\nu}_{2p2h} + \dots \tag{6}$$

In this work we focus on the 1p1h response which, in the RFG model, reads

$$\begin{aligned} W^{\mu\nu}_{1p1h} &= \sum_{ph} \left\langle ph^{-1} \right| \hat{J}^{\mu} \left| F \right\rangle^{*} \left\langle ph^{-1} \right| \hat{J}^{\nu} \left| F \right\rangle \\ &\times \delta(E_p - E_h - \omega)\theta(p - k_F)\theta(k_F - h) \end{aligned} \tag{7}$$

where $|p\rangle \equiv |\mathbf{p}s_p t_p\rangle$ and $|h\rangle \equiv |\mathbf{h}s_h t_h\rangle$ are plane wave states for particles and holes, respectively, and $|F\rangle$ is the RFG ground state with all momenta occupied below the Fermi momentum k_F. The novelty compared to previous works on scaling is that we start from a current operator that is a sum of one-body and two-body operators. This approach allows us to consider the contributions of both the usual electromagnetic current of the nucleon and the meson-exchange currents (MEC) to the 1p1h response:

$$\hat{J}^{\mu} = \hat{J}^{\mu}_1 + \hat{J}^{\mu}_2, \tag{8}$$

where $\hat{J}_1$ represents the one-body (OB) electromagnetic current of the nucleon, while $\hat{J}_2$ is the two-body MEC. Both currents can generate non-zero matrix elements for 1p1h excitation. MEC are two-body operators and they can induce 1p1h excitation due to the interaction of the hit nucleon with a second nucleon acting as a spectator. The many-body matrix elements of these operators are given by

$$\left\langle ph^{-1} \right| \hat{J}^{\mu}_1 \left| F \right\rangle = \langle p| \hat{J}^{\mu}_1 |h\rangle \tag{9}$$

for the OB current and

$$\left\langle ph^{-1} \right| \hat{J}^{\mu}_2 \left| F \right\rangle = \sum_{k<k_F} \left[\langle pk| \hat{J}^{\mu}_2 |hk\rangle - \langle pk| \hat{J}^{\mu}_2 |kh\rangle \right] \tag{10}$$

for the two-body current, where the sum over spectator states (k) is performed over the occupied states in the Fermi gas, considering both the direct and exchange matrix elements. Due to momentum conservation, the matrix element of the OB current between plane waves can be written as

$$\langle p|\hat{J}^{\mu}_1|h\rangle = \frac{(2\pi)^3}{V}\delta^3(\mathbf{q}+\mathbf{h}-\mathbf{p})\frac{m_N}{\sqrt{E_p E_h}} j^{\mu}_1(\mathbf{p},\mathbf{h}), \tag{11}$$

where V is the volume of the system, m_N is the nucleon mass, $E_p = \sqrt{p^2 + m_N^2}$ and $E_h = \sqrt{h^2 + m_N^2}$ are the on-shell energies of the nucleons involved in the process, and $j^{\mu}_1(\mathbf{p},\mathbf{h})$ is the OB current (spin-isospin) matrix

$$j^{\mu}_1(\mathbf{p},\mathbf{h}) = \bar{u}(\mathbf{p})\left(F_1\gamma^{\mu} + i\frac{F_2}{2m_N}\sigma^{\mu\nu}Q_{\nu}\right)u(\mathbf{h}), \tag{12}$$

Preprints (www.preprints.org) | NOT PEER-REVIEWED | Posted: 1 August 2023 doi:10.20944/preprints202308.0066.v1

being F_1 and F_2 the Dirac and Pauli form factors of the nucleon. In the case of the two-body current, the elementary matrix element can be written in a similar form:

$$\begin{aligned}\langle p_1' p_2' | \hat{j}_2^\mu | p_1 p_2 \rangle &= \frac{(2\pi)^3}{V^2}\delta^3(\mathbf{p}_1 + \mathbf{p}_2 + \mathbf{q} - \mathbf{p}_1' - \mathbf{p}_2') \\ &\times \frac{m_N^2}{\sqrt{E_1' E_2' E_1 E_2}} j_2^\mu(\mathbf{p}_1', \mathbf{p}_2', \mathbf{p}_1, \mathbf{p}_2). \end{aligned} \tag{13}$$

Here $j_2^\mu(\mathbf{p}_1', \mathbf{p}_2', \mathbf{p}_1, \mathbf{p}_2)$ is a spin-isospin matrix and it depends on the momenta of the two nucleons in the initial and final state. The two-body current contains the sum of the diagrams shown in Figure 1, including the seagull, pionic, and Δ isobar currents. The specific form of the two-body current function will be given later when we discuss the MEC model. By inserting (13) into Eq. (10) we obtain an expression similar to (11) that resembles the matrix element of an effective one-body (OB) current for the MEC:

$$\left\langle ph^{-1} \middle| \hat{j}_2^\mu \middle| F \right\rangle = \frac{(2\pi)^3}{V}\delta^3(\mathbf{q} + \mathbf{h} - \mathbf{p}) \frac{m_N}{\sqrt{E_p E_h}} j_2^\mu(\mathbf{p}, \mathbf{h}). \tag{14}$$

Here the effective OB current generated by the MEC involves a sum over the spectator nucleons and is defined by

$$\begin{aligned} j_2^\mu(\mathbf{p}, \mathbf{h}) &\equiv \\ &\sum_{k<k_F} \frac{m_N}{V E_k} \left[j_2^\mu(\mathbf{p}, \mathbf{k}, \mathbf{h}, \mathbf{k}) - j_2^\mu(\mathbf{p}, \mathbf{k}, \mathbf{k}, \mathbf{h}) \right]. \end{aligned} \tag{15}$$

Note that in the thermodynamic limit $V \to \infty$ the above sum will be transformed into an integral over the momenta occupied in the Fermi gas:

$$\frac{1}{V}\sum_{k<k_F} \to \sum_{s_k t_k} \int \frac{d^3k}{(2\pi)^3}\theta(k_F - k). \tag{16}$$

Finally, we can write the transition matrix element of the total current between the ground state and the 1p1h state as

$$\left\langle ph^{-1} \middle| \hat{j}^\mu \middle| F \right\rangle = \frac{(2\pi)^3}{V}\delta^3(\mathbf{q} + \mathbf{h} - \mathbf{p}) \frac{m_N}{\sqrt{E_p E_h}} j^\mu(\mathbf{p}, \mathbf{h}), \tag{17}$$

where the effective total current for the 1p1h excitation includes contributions from both the one-body current and MEC:

$$j^\mu(\mathbf{p}, \mathbf{h}) = j_1^\mu(\mathbf{p}, \mathbf{h}) + j_2^\mu(\mathbf{p}, \mathbf{h}). \tag{18}$$

By inserting (17) into Eq. (7) and taking the thermodynamic limit, we obtain the following expression for the hadronic tensor:

$$\begin{aligned} W^{\mu\nu} &= \frac{V}{(2\pi)^3}\int d^3h \delta(E_p - E_h - \omega) \frac{m_N^2}{E_p E_h} 2 w^{\mu\nu}(\mathbf{p}, \mathbf{h}) \\ &\times \theta(p - k_F)\theta(k_F - h), \end{aligned} \tag{19}$$

where $\mathbf{p} = \mathbf{h} + \mathbf{q}$ by momentum conservation after integration over $\mathbf{p}$. The function $w^{\mu\nu}$ is the effective single-nucleon hadronic tensor in the transition

$$w^{\mu\nu}(\mathbf{p}, \mathbf{h}) = \frac{1}{2}\sum_{s_p s_h} j^\mu(\mathbf{p}, \mathbf{h})^* j^\nu(\mathbf{p}, \mathbf{h}). \tag{20}$$

Preprints (www.preprints.org) | NOT PEER-REVIEWED | Posted: 1 August 2023 doi:10.20944/preprints202308.0066.v1

In this equation, we did not include the sum over isospin $t_p = t_h$. Therefore, $w^{\mu\nu}$ refers to the tensor of either proton or neutron emission, and the total tensor would be the sum of the two contributions. Note that the effective single-nucleon tensor $w^{\mu\nu}$ includes the contribution of MEC, thus encompassing an interference between the one-body and two-body currents. Indeed, the relevant diagonal components of the effective single-nucleon hadronic tensor for the longitudinal and transverse responses (4) can be expanded as

$$\begin{aligned} w^{\mu\mu}(\mathbf{p},\mathbf{h}) &= \frac{1}{2}\sum_{s_p s_h} |j_1^\mu + j_2^\mu|^2 \\ &= \frac{1}{2}\sum |j_1^\mu|^2 + \mathrm{Re}\sum (j_1^\mu)^* j_2^\mu + \frac{1}{2}\sum |j_2^\mu|^2 \\ &\equiv w_1^{\mu\mu} + w_{12}^{\mu\mu} + w_2^{\mu\mu} \end{aligned} \tag{21}$$

where $w_1^{\mu\mu}$ is the tensor corresponding to the one-body current, $w_{12}^{\mu\mu}$ represents the interference between the one-body and two-body currents, and $w_2^{\mu\mu}$ corresponds to the contribution of the two-body current alone. The one-body part is the leading contribution in the quasielastic peak, while the dominant contribution of the MEC corresponds to the interference with the one-body current [33,48], being the pure contribution of the two-body current generally smaller.

2.3. Responses in the relativistic mean field approach

Going beyond the Relativistic Fermi Gas (RFG) model, the Relativistic Mean Field (RMF) approach for nuclear matter allows for the inclusion of dynamic relativistic effects. The simplest approximation in this framework is to introduce constant mean scalar and vector potentials with which the nucleons interact [22,23,25,26]. The scalar potential is attractive, while the vector potential is repulsive. The single-particle wave functions still exhibit plane-wave behavior with momentum p in nuclear matter, but with an on-shell energy given by

$$E = \sqrt{m_N^{*2} + p^2}, \tag{22}$$

where m_N^* is the relativistic effective mass of the nucleon, defined as

$$m_N^* = m_N - g_s\phi_0 = M^* m_N. \tag{23}$$

Here ϕ_0 is the scalar potential energy of the RMF and g_s the corresponding coupling constant [23], and $M^* = 0.8$ for ^{12}C, the nucleus considered in this work [44]. To account for the interaction with the vector potential, a positive energy term needs to be added to the on-shell energy. Therefore, the total energy of the nucleon can be expressed as:

$$E_{RMF} = E + E_v. \tag{24}$$

In this work we use the value $E_v = 141$ MeV, obtained in Ref. [44] for ^{12}C. Note that in observables that only depend on the energy differences between initial and final particles, the vector energy cancels out, and only the on-shell energy appears. This cancellation happens, as we will see, in the response associated to the one-body current. However, in the case of the two-body current, the vector energy needs to be taken into account in the Δ current, as we will see in the next section.

In the present RMF approach of nuclear matter, the evaluation of the hadronic tensor is done similarly to the RFG, with the difference that the spinors $u(p)$ now correspond to the solutions of

Preprints (www.preprints.org) | NOT PEER-REVIEWED | Posted: 1 August 2023 doi:10.20944/preprints202308.0066.v1

the Dirac equation with the relativistic effective mass m_N^*. From Eq. (19) the 1p1h nuclear response functions are then given by

$$\begin{aligned} R_K(q,\omega) &= \frac{V}{(2\pi)^3}\int d^3h \frac{(m_N^*)^2}{E_p E_h} 2w_K(\mathbf{p},\mathbf{h}) \\ &\times\theta(p-k_F)\theta(k_F-h)\delta(E_p-E_h-\omega), \end{aligned} \tag{25}$$

where E_p, E_h are the on-shell energies with effective mass m_N^*, and w_K are the single-nucleon responses for the 1p1h excitation

$$w_L = w^{00}, \qquad w_T = w^{11}+w^{22}. \tag{26}$$

The effective single-nucleon tensor $w^{\mu\nu}$ is constructed as in Eq. (20), but the current is obtained from matrix elements using spinors with the relativistic effective mass m_N^* instead of the normal nucleon mass. This prescription is also followed when evaluating the 1p1h matrix elements of the MEC (as discussed in the next section).

To compute the integral (25), we change to the variables (E_h, E_p, ϕ), using $h^2 dh d\cos\theta = (E_h E_p/q) dE_h dE_p$. Then the integral over E_p can be performed using the Dirac delta. This fixes the angle θ_h between $\mathbf{q}$ and $\mathbf{h}$

$$\cos\theta_h = \frac{2E_h\omega + Q^2}{2hq}. \tag{27}$$

The integration over the angle ϕ gives 2π by symmetry of the responses when $\mathbf{q}$ is on the z-axis [14]. The result is an integral over the initial nucleon energy

$$R_K(q,\omega) = \frac{V}{(2\pi)^3}\frac{2\pi m_N^{*3}}{q}\int_{\epsilon_0}^{\infty} d\epsilon\, n(\epsilon)\, 2w_K(\epsilon,q,\omega), \tag{28}$$

where we have defined the adimensional energies $\epsilon = E_h/m_N^*$ and $\epsilon_F = E_F/m_N^*$. Moreover we have introduced the energy distribution of the Fermi gas $n(\epsilon) = \theta(\epsilon_F - \epsilon)$. The lower limit of the integral (28), ϵ_0, represents the minimum energy that an on-shell nucleon can have when it absorbs energy ω and momentum q [14]

$$\epsilon_0 = \text{Max}\left\{\kappa\sqrt{1+\frac{1}{\tau}} - \lambda, \epsilon_F - 2\lambda\right\}, \tag{29}$$

where we have defined the dimensionless variables

$$\lambda = \frac{\omega}{2m_N^*}, \qquad \kappa = \frac{q}{2m_N^*}, \qquad \tau = \kappa^2 - \lambda^2. \tag{30}$$

From Eq. (28) the nucleons that contribute to the response function $R_K(q,\omega)$ are those with energy ranging from ϵ_0 to ϵ_F. For fixed values of ϕ, q, ω, the integral over energy ϵ in Eq. (28) corresponds to integrating the single nucleon response over a path in the momentum space of the hole $\mathbf{h}$, weighted with the momentum distribution. The angle between $\mathbf{h}$ and $\mathbf{q}$ for each energy is given by Eq. (27). The minimum momentum h_0 correspond to the minimum energy ϵ_0. Indeed, for a specific value of ω, the lower limit of the integral becomes $h = 0$ or $\epsilon_0 = 1$, which corresponds to the center of the quasielastic peak. Using Eq. (29), it is straightforward to verify that this point corresponds to $\lambda = \tau$ in the regime without Pauli blocking.

2.4. Scaling

Scaling is based on the approximated factorization of an averaged single-nucleon response from the nuclear cross section. This factorization is exact in the RMF model with the OB current. In previous works, analytical expressions were obtained from the RFG and RMF models by explicit integration of

Preprints (www.preprints.org) | NOT PEER-REVIEWED | Posted: 1 August 2023 doi:10.20944/preprints202308.0066.v1

the one-body responses, Eq. (28). However in this case, it is not possible to perform the integration (28) analytically because now w_K includes also the matrix elements of the two-body operator. Nevertheless, we can still define averaged single-nucleon responses as

$$\overline{w}_K(q,\omega) = \frac{\int_{\epsilon_0}^{\infty} d\epsilon\, n(\epsilon) w_K(\epsilon,q,\omega)}{\int_{\epsilon_0}^{\infty} d\epsilon\, n(\epsilon)} \tag{31}$$

and we can rewrite Eq. (28) in the form

$$R_K(q,\omega) = \frac{V}{(2\pi)^3}\frac{2\pi m_N^{*3}}{q} 2\overline{w}_K(q,\omega)\int_{\epsilon_0}^{\infty} d\epsilon\, n(\epsilon). \tag{32}$$

The averaged single-nucleon responses, $\overline{w}_K(q,\omega)$, include the combined effect of both the OB current and the MEC in all the 1p1h excitations compatible with given values of (q,ω). Eq. (32) shows that in the RMF model (or the RFG model for effective mass $M^* = 1$) the nuclear responses factorize as the product of the averaged single-nucleon response (including MEC) and the scaling function. In fact a superscaling function can be defined as

$$f^*(\psi^*) = \frac{3}{4}\frac{1}{\epsilon_F - 1}\int_{\epsilon_0}^{\infty} n(\epsilon) d\epsilon, \tag{33}$$

where $\epsilon_F - 1$ is the kinetic Fermi energy in units of m_N^* and the ψ^*-scaling variable is related to the minimum nucleon energy, ϵ_0, as

$$\psi^* = \sqrt{\frac{\epsilon_0 - 1}{\epsilon_F - 1}}\,\mathrm{sgn}(\lambda - \tau). \tag{34}$$

The scaling variable, ψ^*, is negative (positive) for $\lambda < \tau$ ($\lambda > \tau$). In the RMF the scaling function is easily evaluated from Eq. (33), giving

$$f^*(\psi^*) = \frac{3}{4}(1 - \psi^{*2})\theta(1 - \psi^{*2}). \tag{35}$$

Note that the scaling function of nuclear matter is zero for $\epsilon_0 > \epsilon_F$, and this is equivalent to $|\psi^*| > 1$. This is a consequence of the maximum momentum k_F for the nucleons in nuclear matter, which implies that $\epsilon_0 < \epsilon_F$.

Using $V/(2\pi)^3 = N/(\frac{8}{3}\pi k_F^3)$ for nuclear matter we can write the response functions (32) as

$$R_K(q,\omega) = \frac{\epsilon_F - 1}{m_N^* \eta_F^3 \kappa}(Z\overline{w}_K^p(q,\omega) + N\overline{w}_K^n(q,\omega)) f^*(\psi^*), \tag{36}$$

where we have added the contribution of Z protons and N neutrons to the response functions, and $\eta_F = k_F/m_N^*$.

*2.5. SuSAM**

The expression given by Eq (36) for the response function is formally the same as the response in the RMF, the only difference being that the averaged single-nucleon response now includes the contribution of MEC to the 1p1h excitation. This equation, valid for the RMF, serves as the starting point for performing the superscaling analysis with relativistic effective mass (SuSAM*) using electron scattering data, extending the formula to the region $\epsilon_0 > \epsilon_F$ or $|\psi^*| > 1$. We will follow the procedure suggested by Casale *et al.* [57].

In the Fermi gas, it is not possible to extend the averaging formula for $\epsilon_0 > \epsilon_F$ because the momentum distribution is zero and the denominator in (31) vanishes. Therefore, what we do is slightly modify the Fermi gas distribution by allowing a smeared Fermi surface, so that the distribution is not

Preprints (www.preprints.org) | NOT PEER-REVIEWED | Posted: 1 August 2023 doi:10.20944/preprints202308.0066.v1

exactly zero above k_F, allowing for the averaging procedure. By substituting the Fermi distribution with a distribution that is not significantly different from the original one for $h < k_F$, the average of the single-nucleon response will not change significantly in the Fermi gas region $|\psi^*| < 1$.

By this method, the extension of the single-nucleon average is done smoothly and continuously to the region $|\psi^*| > 1$, with the added meaning that, in this way, we are taking into account, at least partially, the high-momentum distribution. This is because it is primarily the nucleons with momenta greater than k_F that contribute to this region. A possible distribution that can be used to extend the averaging procedure is the Fermi distribution:

$$n(h) = \frac{a}{1 + e^{(h-k_F)/b}}. \tag{37}$$

Using this distribution, the integrals in the numerator and denominator of Eq (31) extend to infinity and are well-defined for $\epsilon_0 > \epsilon_F$ or $|\psi^*| > 1$. An appropriate value for the smearing parameter is $b = 50$ MeV/c, used in ref. [57], where the averaged single-nucleon responses were evaluated for the one-body current, and it was found to yield practically the same results as the analytically calculated responses in the strict Fermi gas region. The averaged responses were also found to be very similar to the traditionally extrapolated responses outside this region. This proposed method provides a simple approach that allows for the definition of generalized scaling, including the MEC, consistently, and also takes into account that the nucleons are not limited by a maximum Fermi momentum.

Several approaches exist to obtain a phenomenological scaling function. Different methods are based on different assumptions for the scaling function or the single-nucleon response, but all are ultimately adjusted to experimental data. The original SuSA model, based on the RFG, was fitted to the scaling data of the longitudinal response, to obtain a longitudinal scaling function, f_L, while in the extended SuSA-v2 approach, the RMF model for finite nuclei was used to obtain a transverse scaling function, f_T . The SuSAM* model, based on the nuclear matter RMF with effective mass, directly fitted the quasielastic data of the cross section after discarding the non-scaling data points, to obtain a single phenomenological scaling function valid for both the L and T channels [19].

In the generalized SuSAM* model proposed here, we will follow the same procedure as described in references [42, 43]. First, we subtract the calculated inclusive cross section for two-particle emission in the RMF with a relativistic MEC model from the (e,e') data. This subtraction aims to partially remove the contribution of 2p2h processes present in the data, in order to isolate the purely quasielastic data as much as possible. Next, we will scale each residual data point by dividing it by the contribution of the single nucleon to the cross section, as given by Eq. (36),

$$f^*_{exp} = \frac{\left(\frac{d\sigma}{d\Omega d\omega}\right)_{exp} - \left(\frac{d\sigma}{d\Omega d\omega}\right)_{2p2h}}{\sigma_M(v_L r_L + v_T r_T)}, \tag{38}$$

where the single nucleon cross section includes the averaged single-nucleon responses including MEC

$$r_K = \frac{\epsilon_F - 1}{m^*_N \eta^3_F \kappa}(Z\overline{w}^p_K(q,\omega) + N\overline{w}^n_K(q,\omega)). \tag{39}$$

In the results section, we will proceed with the scaling analysis for the obtained f^*_{exp} data, by a plot as a function of ψ^*, calculated using Eq. (34). This analysis includes a selection process to identify the data points that are most likely to be quasielastic (which exhibit approximate scaling behavior) and discarding the remaining data points (mainly non-scaling inelastic processes). Finally, we will fit a phenomenological scaling function to the surviving data points, aiming to describe the global scaling behavior of the quasielastic region.

Preprints (www.preprints.org) | NOT PEER-REVIEWED | Posted: 1 August 2023 doi:10.20944/preprints202308.0066.v1

2.6. Meson-exchange currents

In this work, we use the relativistic meson exchange currents (MEC) model described in Ref. [43]. The Feynman diagrams shown in Figure 1 illustrate the different components of the MEC model. Diagrams (a) and (b) correspond to the seagull current, diagram (c) represents the pion-in-flight current, and diagrams (d,e) and (f,g) depict the forward- and backward- $\Delta(1232)$ currents, respectively. The specific treatment of the Δ current is model-dependent, and various versions exist with possible corrections to the off-shell relativistic interaction of the Δ. Other widely used models for MEC include those described in Refs. [33,42,58].

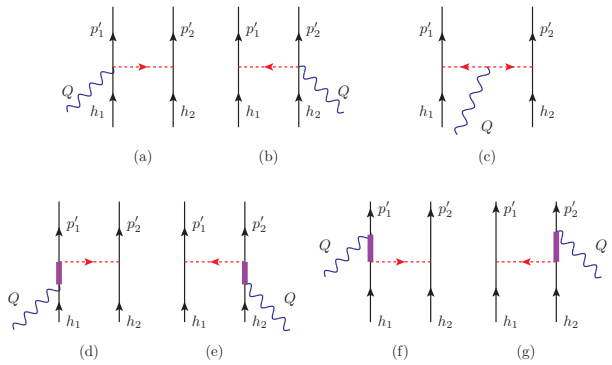

Figure 1. Feynman diagrams for the 2p2h MEC model used in this work.

While these different models may exhibit slight variations and corrections to the Δ off-shell interaction, they generally yield similar results for the dominant transverse response at the quasielastic peak. In particular, in the results section, we will compare our findings with the model presented in Refs. [33,58], which we previously employed to assess the impact of MEC on the 1p1h response.

In our model the MEC functions defined in Eq. (13) correspond to the sum of diagrams of Figure 1

$$j_2^\mu(\mathbf{p}_1', \mathbf{p}_2', \mathbf{p}_1, \mathbf{p}_2) = j_{sea}^\mu + j_\pi^\mu + j_\Delta^\mu, \tag{40}$$

where the Δ current is the sum of forward and backward terms

$$j_\Delta^\mu = j_{\Delta F}^\mu + j_{\Delta B}^\mu. \tag{41}$$

These functions are defined by

$$j_{sea}^\mu = [I_z]_{t_1' t_2', t_1 t_2} \frac{f^2}{m_\pi^2} V_{\pi NN}^{s_1' s_1}(p_1', p_1) F_{\pi NN}(k_1^2) \bar{u}_{s_2'}(p_2') F_1^V \gamma^5 \gamma^\mu u_{s_2}(p_2) + (1 \leftrightarrow 2) \tag{42}$$

$$j_\pi^\mu = [I_z]_{t_1' t_2', t_1 t_2} \frac{f^2}{m_\pi^2} F_1^V V_{\pi NN}^{s_1' s_1}(p_1', p_1) V_{\pi NN}^{s_2' s_2}(p_2', p_2)(k_1^\mu - k_2^\mu) \tag{43}$$

$$j_{\Delta F}^\mu = [U_z^F]_{t_1' t_2', t_1 t_2} \frac{f f^*}{m_\pi^2} V_{\pi NN}^{s_2' s_2}(p_2', p_2) F_{\pi N\Delta}(k_2^2) \bar{u}_{s_1'}(p_1') k_2^\alpha G_{\alpha\beta}(p_1 + Q) \Gamma^{\beta\mu}(Q) u_{s_1}(p_1) + (1 \leftrightarrow 2) \tag{44}$$

$$j_{\Delta B}^\mu = [U_z^B]_{t_1' t_2', t_1 t_2} \frac{f^2 f^*}{m_\pi^2} V_{\pi NN}^{s_2' s_2}(p_2', p_2) F_{\pi N\Delta}(k_2^2) \bar{u}_{s_1'}(p_1') k_2^\beta \hat{\Gamma}^{\mu\alpha}(Q) G_{\alpha\beta}(p_1' - Q) u_{s_1}(p_1) + (1 \leftrightarrow 2) \tag{45}$$

We will evaluate these matrix elements in the framework of the RMF model, where the spinors $u(p)$ are the solutions of the Dirac equation with relativistic effective mass m_N^*. The four-vectors $k_i^\mu = p_i'^\mu - p_i^\mu$ with $i = 1, 2$ are the momenta transferred to the nucleons 1,2. We have defined the following function that includes the πNN vertex, a form factor, and the pion propagator

$$V_{\pi NN}^{s_1' s_1}(p_1', p_1) = F_{\pi NN}(k_1^2) \frac{\bar{u}(p_1') \gamma^5 \not{k}_1 u(p_1)}{k_1^2 - m_\pi^2}. \tag{46}$$

Preprints (www.preprints.org) | NOT PEER-REVIEWED | Posted: 1 August 2023 doi:10.20944/preprints202308.0066.v1

We apply strong form factors at the pion absorption/emission vertices given by [35,59]

$$F_{\pi NN}(k) = F_{\pi N\Delta}(k) = \frac{\Lambda^2 - m_\pi^2}{\Lambda^2 - k^2}. \tag{47}$$

The charge structure of the MEC involves the isospin matrix element of the operators

$$I_z = i[\tau(1) \times \tau(2)]_z, \tag{48}$$

$$U_z^F = \sqrt{\frac{3}{2}} \sum_{i=1}^{3} (T_i T_z^\dagger) \otimes \tau_i, \tag{49}$$

$$U_z^B = \sqrt{\frac{3}{2}} \sum_{i}^{3} (T_z T_i^\dagger) \otimes \tau_i, \tag{50}$$

where we denote by $T_i^\dagger$ the Cartesian coordinates of the $\frac{1}{2} \to \frac{3}{2}$ transition isospin operator, defined by its matrix elements [60]

$$\langle \tfrac{3}{2} t_\Delta | T_\mu^\dagger | \tfrac{1}{2} t \rangle = \langle \tfrac{1}{2} t 1 \mu | \tfrac{3}{2} t_\Delta \rangle \tag{51}$$

$T_\mu^\dagger$ being the spherical components of the vector $\vec{T}^\dagger$. With the aid of the expression $T_i T_j^\dagger = (2/3)\delta_{ij} - \frac{i}{3}\tau_i \tau_j$ and making the summation, we can rewrite the isospin operators in the forward and backward Δ current as

$$U_z^F = \sqrt{\frac{3}{2}} \left(\frac{2}{3} \tau_z^{(2)} - \frac{i}{3} \left[\tau^{(1)} \times \tau^{(2)} \right]_z \right) \tag{52}$$

$$U_z^B = \sqrt{\frac{3}{2}} \left(\frac{2}{3} \tau_z^{(2)} + \frac{i}{3} \left[\tau^{(1)} \times \tau^{(2)} \right]_z \right). \tag{53}$$

The $\gamma N \to \Delta$ transition vertex in the forward Δ current is defined as [61,62]

$$\Gamma^{\beta\mu}(Q) = \frac{C_3^V}{m_N} (g^{\beta\mu} \not{Q} - Q^\beta \gamma^\mu) \gamma_5 \tag{54}$$

while for the backward Δ current

$$\hat{\Gamma}^{\mu\alpha}(Q) = \gamma^0 [\Gamma^{\alpha\mu}(-Q)]^\dagger \gamma^0. \tag{55}$$

In this vertex we have neglected contributions of order $O(1/m_N^2)$. Note that the $\Gamma^{\beta\mu}$ operator is a spin matrix and depends on the vector form factor C_3^V. In this paper, we use the vector form factor in Δ current from Refs. [40,62]:

$$C_3^V(Q^2) = \frac{2.13}{(1 - \frac{Q^2}{M_V^2})^2} \frac{1}{1 - \frac{Q^2}{4M_V^2}}. \tag{56}$$

Various alternative approximations to the propagator have been proposed [63]. However, in the case of the quasielastic peak, the typical kinematics are of the order of 1 GeV, and these issues are not expected to be relevant. They are overshadowed by other more significant nuclear effects that dominate in this energy regime. Here we use the Δ propagator commonly used for the spin-3/2 field

$$G_{\alpha\beta}(P) = \frac{\mathcal{P}_{\alpha\beta}(P)}{P^2 - M_\Delta^2 + i M_\Delta \Gamma(P^2) + \frac{\Gamma(P^2)^2}{4}} \tag{57}$$

Preprints (www.preprints.org) | NOT PEER-REVIEWED | Posted: 1 August 2023 doi:10.20944/preprints202308.0066.v1

where M_Δ and Γ are the Δ mass and width respectively. The projector $\mathcal{P}_{\alpha\beta}(P)$ over spin-3/2 on-shell particles is given by

$$\begin{aligned}\mathcal{P}_{\alpha\beta}(P) &= -(\not{P} + M_\Delta) \\ &\times \left[g_{\alpha\beta} - \frac{\gamma_\alpha \gamma_\beta}{3} - \frac{2P_\alpha P_\beta}{3M_\Delta^2} + \frac{P_\alpha \gamma_\beta - P_\beta \gamma_\alpha}{3M_\Delta} \right].\end{aligned} \tag{58}$$

Finally, the Δ width $\Gamma(P^2)$ is given by

$$\Gamma(P^2) = \Gamma_0 \frac{m_\Delta}{\sqrt{P^2}} \left(\frac{p_\pi}{p_\pi^{res}} \right)^3. \tag{59}$$

In the above equation, p_π is the momentum of the final pion resulting from the Δ decay an p_π^{res} is its value at resonance ($P^2 = m_\Delta^2$), and $\Gamma_0 = 120$ MeV is the width at rest. The width (59) corresponds to the Δ in vacuum, and it is expected to be slightly different in the medium depending on the kinematics. One could investigate the dependence of the results on the choice of the width. However, in this work, we do not delve into this issue because, as we will see, the effect of the MEC on the 1p1h response is generally small, and corrections due to fine-tuning of the model are unlikely to substantially alter the results.

In the relativistic mean field description used in this work, we consider that the Δ is also interacting with scalar and vector fields, acquiring an effective mass and vector energy. To treat this case, we make the following substitutions in the Δ propagator for the Δ mass and momentum [25,64]:

$$M_\Delta \to M_\Delta^*, \qquad P^{*\mu} = P^\mu - \delta_{\mu 0} E_v^\Delta. \tag{60}$$

We use the value $M_\Delta^* = 1042$ MeV, taken from [45], and the universal vector coupling $E_v^\Delta = E_v$.

With the MEC current defined in Eqs. (24-27), the effective one-body current $j_2(\mathbf{p}, \mathbf{h})$ is generated by summing over the spin, isospin and momentum of the spectator nucleon, as in Eq. (15). First, it can be observed that due to the sum over isospin t_k, the direct term is zero (see Ref. [33] for details). Therefore, the many-body diagrams that contribute to the 1p1h MEC are those shown in Figure 2. Furthermore, it can be verified that diagrams e and f are also zero. Therefore, only diagrams a, b, c, and d survive and contribute to the 1p1h MEC matrix elements.

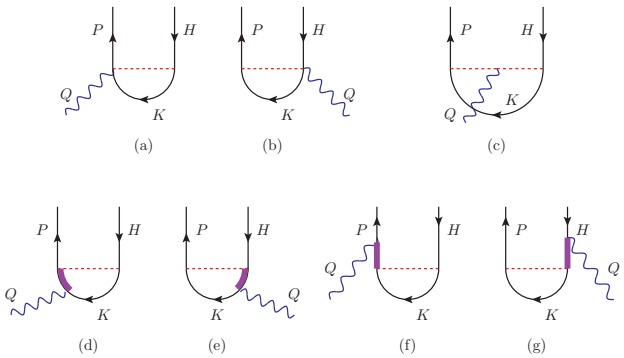

Figure 2. Diagrams for the 1p1h MEC matrix elements

3. Results

In this section, we present results for the effects of MEC on the 1p1h response functions using several models: the relativistic Fermi gas, the relativistic mean field, and the generalized SuSAM* model. By employing these different models, we take into account relativistic kinematics and we can analyze the impact of including the relativistic effective mass of the nucleon and the Δ resonance appearing in the MEC. The scaling analysis described in the previous Section will allow us to study the

Preprints (www.preprints.org) | NOT PEER-REVIEWED | Posted: 1 August 2023 doi:10.20944/preprints202308.0066.v1

influence of MEC on the generalized scaling function also in the region $|\psi^*| > 1$ where the RFG and RMF responses are zero. Moreover, we can investigate how the inclusion of MEC affects the scaling function and compare it with the predictions of the RFG and RMF models.

Unless stated otherwise, we present the results for ^{12}C with a Fermi momentum of $k_F = 225$ MeV/c. We use an effective mass of $M^* = 0.8$, following the same choice of parameters as in reference [44,45]. The calculation of 1p1h responses involves evaluating the 1p1h matrix element of the MEC, as given by Eq (15). This requires performing a numerical three-dimensional integration to account for the momentum dependence. Subsequently, a one-dimensional integration is carried out to calculate the averaged single-nucleon responses, as described in Eq (31).

First, since this work is an extension of the MEC model from Ref. [33] to the superscaling formalism, we will compare with the OB-MEC interference responses presented in [33] within the framework of the RFG. It should be noted that in [33] a different version of the Δ current was used. The Δ current was obtained from the $\gamma N\Delta$ Lagrangian proposed by Pascalutsa [58]

$$\mathcal{L}_{\gamma N\Delta} = ie\frac{G_1}{2m_N}\overline{\psi}^{\alpha}\Theta_{\alpha\mu}\gamma_\nu\gamma_5 T_3^\dagger N F^{\nu\mu} + \text{h.c.}, \tag{61}$$

plus $O(1/m_N^2)$ terms that give negligible contribution in the quasielastic energy region. The tensor $\Theta_{\alpha\mu}$ may contain an off-shell parameter and another arbitrary parameter related to the contact invariance of the Lagrangian. In this work we use the simplest form

$$\Theta_{\alpha\mu} = g_{\alpha\mu} - \frac{1}{4}\gamma_\alpha\gamma_\mu. \tag{62}$$

The coupling constant G_1 was determined in [58] by fitting Compton scattering on the nucleon. However, there is a detail that needs to be clarified: the isospin operator used by Pascalutsa is normalized differently from the standard convention. That is, $T_i^{\text{Pascalutsa}} = \sqrt{\frac{3}{2}}T_i$, where T_i is the operator used in our calculation. This means that if we use the standard T_i in the Lagrangian (61), it should be multiplied by $\sqrt{\frac{3}{2}}$. This is equivalent to multiplying Pascalutsa's coupling constant $G_1 = 4.2$ by the factor $\sqrt{\frac{3}{2}}$. In reference [33], this detail went unnoticed, and the $\sqrt{3/2}$ factor was not included in the calculations.

Using the Lagrangian given by Eq. (61), the following Δ current is obtained:

$$\begin{aligned} j^\mu_{\Delta F} &= [(T_i T_3^\dagger)\otimes\tau_i]_{t_1' t_2', t_1 t_2}\frac{ff^*}{m_\pi^2}F_\Delta(Q^2)V^{s_2' s_2}_{\pi NN}(p_2', p_2)F_{\pi N\Delta}(k_2^2) \\ &\quad \bar{u}_{s_1'}(p_1')k_2^\alpha\left[\Theta^{\alpha\beta}G_{\beta\rho}(p_1+Q)\frac{G_1}{2m_N}[\Theta^{\rho\mu}\gamma^\nu - \Theta^{\rho\nu}\gamma^\mu]\gamma_5 Q_\nu\right]u_{s_1}(p_1) + (1\leftrightarrow 2) \end{aligned} \tag{63}$$

and a similar expression for the Δ backward current. This current was used in Ref. [33] to compute the OB-MEC interference with the following form factor

$$F_\Delta(Q^2) = G_E^p(Q^2)\left(1 - \frac{Q^2}{3.5(GeV/c)^2}\right)^{-1/2} \tag{64}$$

where G_E^p is the electric form factor of the proton.

In Figure 3, we present the interference between the OB and Δ currents in the transverse response of ^{40}Ca. We compare our results with the model of reference [33] in RFG, where the Lagrangian of Pascalutsa was used. The results of [33] have been corrected with the factor of $\sqrt{\frac{3}{2}}$ mentioned earlier. For $q = 500$ MeV/c, there is little difference between the two models. However, for $q = 1$ GeV/c, the difference becomes more noticeable.

Preprints (www.preprints.org) | NOT PEER-REVIEWED | Posted: 1 August 2023 doi:10.20944/preprints202308.0066.v1

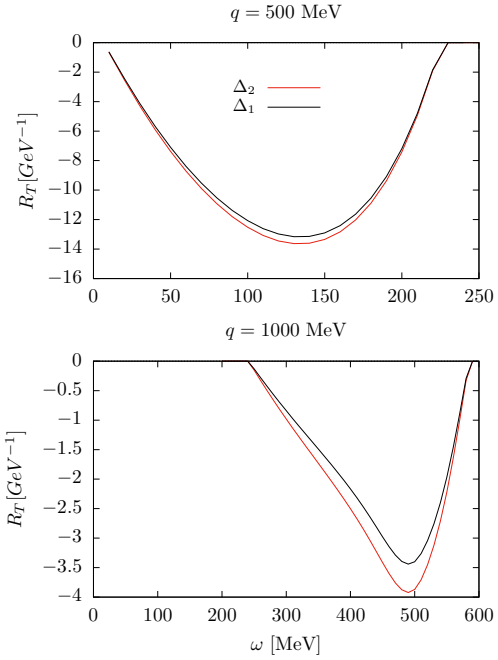

Figure 3. Interference OB-MEC in the transverse response of ^{40}Ca for two values of the momentum transfer, with $k_F = 237$ MeV/c. In the graph, the curve labeled Δ_1 corresponds to using the Δ current of the present work in RFG. The curve Δ_2 corresponds to the calculation from reference [33].

The results of Figure 3 show that the Δ current model used in this work does not differ significantly from the model in reference [33], providing similar results. The small differences observed can be attributed to the different form factor and coupling constants, and can be understood as a model dependence in these results. From here on, all the results refer to the Δ current model described in the equations (44,45).

It is expected that any relativistic model should reproduce the results of the well-established non-relativistic model for small values of energy and momentum in the non-relativistic limit [65]. As a check in this regard, in Figure 4 we compare the present model with the non-relativistic Fermi gas model from ref. [48]. The non relativistic Δ current used is taken from [33]. To perform this comparison the same form factors and coupling constants are used in the relativistic and non relativistic models. To take this limit in Figure 4, we follow the procedure as follows: q is small and $k_F = q/2$. We show the comparison between the two models for various values of q ranging from 100 to 500 MeV/c. In the left panels, we present the contribution of the transverse response stemming from the interference OB-π between the pure pionic MEC (diagrams a-c in Figure 2) and in the right panels we show the OB-Δ interference (diagrams d-g in Figure 2) for the same values of q. As expected, we observe that for $q = 100$ MeV/c, the relativistic and non-relativistic models practically coincide, demonstrating the consistency between the two models in the non-relativistic limit.

In Figure 4 one can also observe that for low values of q the dominant contributions to the MEC are from the seagull and pion-in-flight diagrams, with the seagull diagram playing a particularly important role. These diagrams contribute positively to the MEC, enhancing the overall response. On the other hand, the contribution from the Δ resonance is negative. As q increases, the influence of the Δ resonance becomes more significant, and it starts to dominate the MEC contribution for q values around 400 MeV/c.

Preprints (www.preprints.org) | NOT PEER-REVIEWED | Posted: 1 August 2023 doi:10.20944/preprints202308.0066.v1

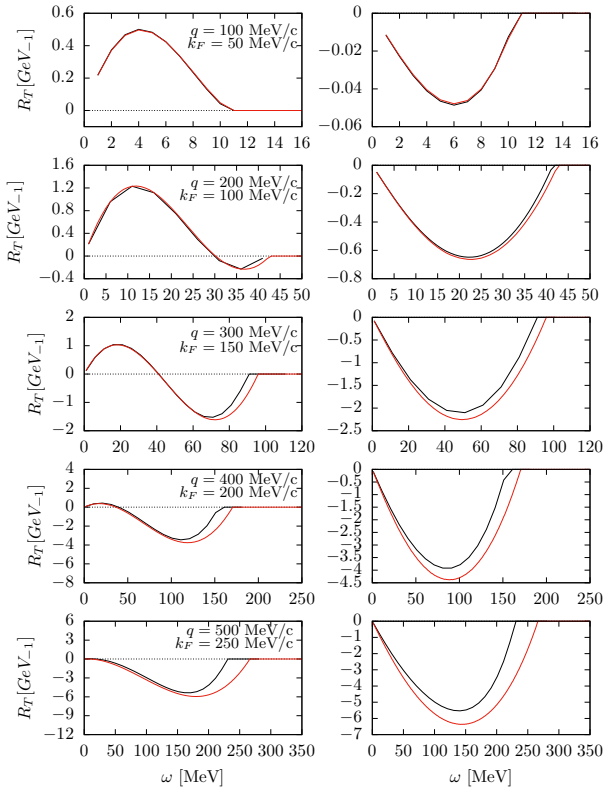

Figure 4. Comparison between relativistic and non relativistic MEC transverse responses in ^{12}C. Black lines: RFG. Red lines: non-relativistic Fermi gas. Left panels show the interference OB-π, and left panels the interference OB-Δ. In these calculations the strong form factors in the pion vertices are set to one.

Before performing the scaling analysis, we examine the averaged single-nucleon responses that will be used to scale the data. In Figure 5, we display the longitudinal and transverse single-nucleon responses for various values of q as a function of the scaling variable. The calculated responses are shown separately for the OB current and the total responses including the MEC and taking into account the sum of protons and neutrons. The total response, which we have defined in equation (36), comes from the product of the single nucleon with the phenomenological scaling function obtained from the (e, e') data as shown below. We have used a Fermi distribution, Eq.(37), with a smearing parameter $b = 50 MeV/c$, although the single nucleon responses do not depend much on this specific value. It is observed that the effect of the MEC is negligible in the longitudinal response, as the curves for the OB current and total response overlap. However, in the transverse response, the effect of the MEC becomes appreciable, resulting in a reduction of the w_T response compared to the OB current. This reduction can be attributed to the interference between the one-body and two-body currents, which leads to a modified transverse response. The comparison between the OB current and the total response including the MEC provides insights into the contributions of the MEC to the single-nucleon responses and sets the stage for the subsequent scaling analysis.

Preprints (www.preprints.org) | NOT PEER-REVIEWED | Posted: 1 August 2023 doi:10.20944/preprints202308.0066.v1

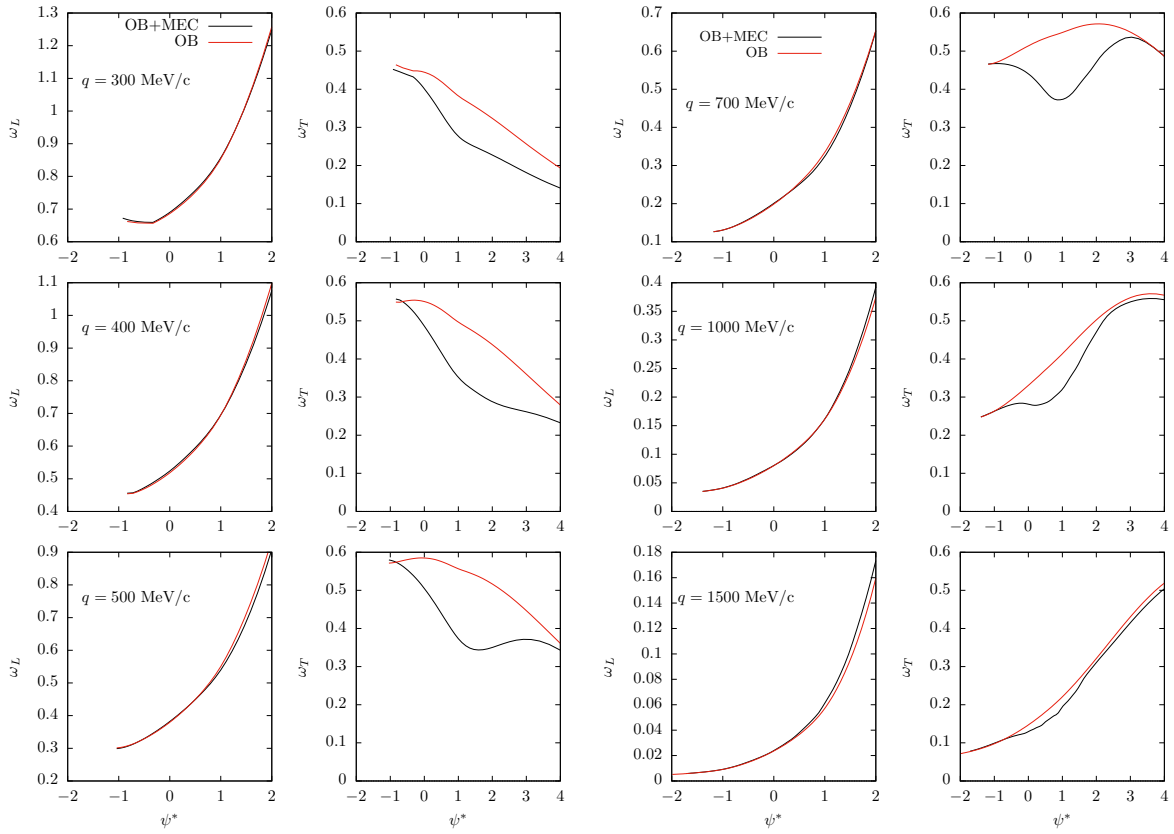

Figure 5. Averaged single nucleon responses computed with and without MEC, for several values of the momentum transfer as a function of the scaling variable ψ^*.

Note that the center of the quasielastic peak corresponds to $\psi^* = 0$, where the energy and momentum can be transferred to a nucleon at rest. We see that MEC have a larger impact in the region $\psi^* > 0$, that is, the right-hand side of the peak, corresponding to higher energy transfers.

In Figure 6, we present the scaling analysis of the ^{12}C data. In the top panel, the experimental data, f^*_{exp}, are plotted against ψ^* in the interval $-2 < \psi^* < 2$. Experimental data are from Refs. [66,67] and cover a wide electron energy range, from 160 MeV up to 5.8 GeV. We observe a significant dispersion of many data points, indicating a wide range of inelastic scattering events. However, we also notice that a portion of the data points cluster together and collapse into a thick band. These data points can be considered as associated to quasielastic (1p1h) events. To select these quasielastic data, we apply a density criterion. For each point, we count the number of points, n, within a neighborhood of radius $r = 0.1$, and eliminate the point if n is less than 25. Points that have been disregarded are likely to correspond to inelastic excitations and low energy processes that violate scaling and cannot be considered within quasielastic processes. We observe that the remaining selected points, about half of the total, shown in the middle panel of Figure 6, form a distinct thick band. These points represent the ones that best describe the quasielastic region and approximately exhibit scaling behavior. The red curve represents the phenomenological quasielastic function $f^*(\psi^*)$, that provides the best fit to the selected data using a sum of two Gaussian functions:

$$f^*(\psi^*) = a_3 e^{-(\psi^* - a_1)^2/(2a_2^2)} + b_3 e^{-(\psi^* - b_1)^2/(2b_2^2)}. \tag{65}$$

The parameters found are shown in Table 1.

Preprints (www.preprints.org) | NOT PEER-REVIEWED | Posted: 1 August 2023 doi:10.20944/preprints202308.0066.v1

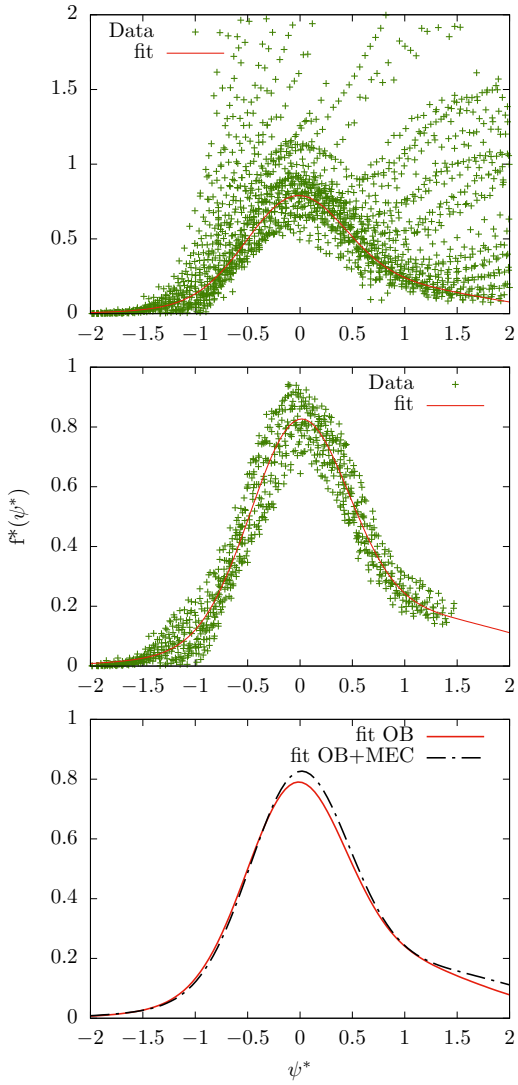

Figure 6. Scaling analysis of ^{12}C data including MEC and relativistic effective mass $M^* = 0.8$. The Fermi momentum is $k_F = 225$ MeV/c. In the top panel, we show the data points after scaling, representing the overall distribution. In the middle panel, we display the selected data points, which have been chosen after eliminating those that do not exhibit clear scaling behavior. In the bottom panel, we present the phenomenological scaling function, which has been fitted to the selected data points, compared to the scaling function obtained in a similar analysis without MEC. Experimental data are taken from Refs. [66,67].

Table 1. Table of fitted parameters of the scaling function.

a_1	a_2	a_3	b_1	b_2	b_3
−0.01015	0.46499	0.69118	0.86952	1.16236	0.17921

In the bottom panel of Figure 6 we compare the scaling function obtained in our analysis with the scaling function obtained without including the MEC contributions. When including the MEC, the scaling function appears slightly higher since the single-nucleon response with MEC is slightly smaller than without them. However, both analyses provide a similarly acceptable description of the data. This suggests that while the MEC do have an impact on the scaling behavior, their effect is relatively small and does not significantly alter the overall scaling pattern observed in the data.

Preprints (www.preprints.org) | NOT PEER-REVIEWED | Posted: 1 August 2023 doi:10.20944/preprints202308.0066.v1

Now that we have obtained the phenomenological scaling function through the scaling analysis, we can utilize this function to calculate the response functions of the model beyond the RMF. By multiplying the scaling function by the averaged single nucleon responses, as stated in Eq (36), we can extend our calculations to different kinematic regimes and explore the behavior of the responses beyond the relativistic mean field description. This allows us to investigate the influence of various factors, such as the MEC and relativistic effects, on the response functions and cross sections.

In Figures 7–10, we present the interferences of the OB-MEC in the response functions for different values of q (500, 700, 1000, and 1500 MeV/c). We separate the interferences into OB-seagull, OB-pionic, and OB-Δ contributions for both the longitudinal and transverse responses as functions of ω. Each panel displays three curves corresponding to the free RFG (with effective mass $M^* = 1$), the RMF (with effective mass $M^* = 0.8$), and the present SuSAM* model. These figures allow us to analyze the relative contributions of the different OB-MEC interferences in the response functions at various kinematic regimes. By comparing the results obtained from the RFG, RMF, and SuSAM* models, we can observe the effects of including the relativistic interaction through the effective mass and the scaling function on the interferences.

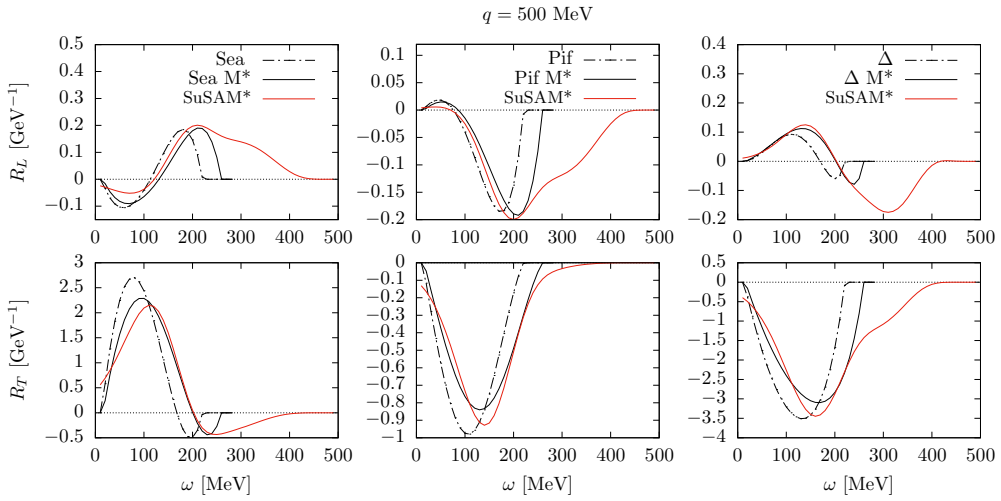

Figure 7. Interference OB-MEC responses separated in seagull, pion-in-flight, and Δ contributions for ^{12}C and $q = 500$ MeV/c. In each panel we compare the results of RFG (with $M^* = 1$, dot-dash), with the RMF (with $M^* = 0.8$) and the SuSAM* model.

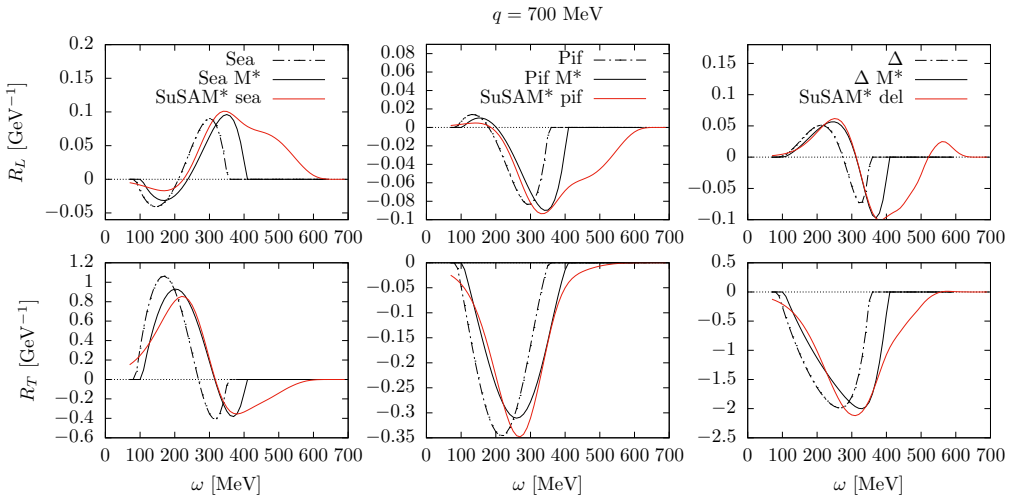

Figure 8. The same as Figure 7 for $q = 700$ MeV/c.

Preprints (www.preprints.org) | NOT PEER-REVIEWED | Posted: 1 August 2023 doi:10.20944/preprints202308.0066.v1

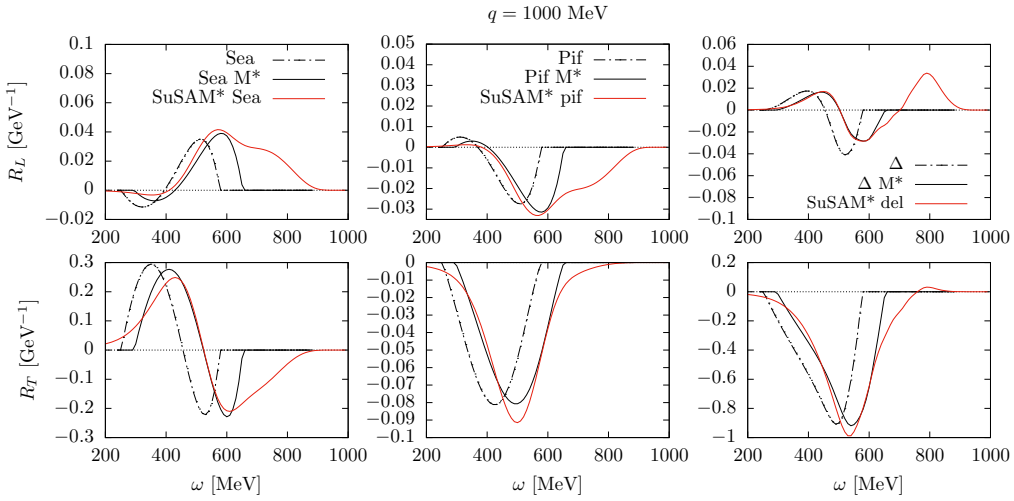

Figure 9. The same as Figure 7 for $q = 1000$ MeV/c.

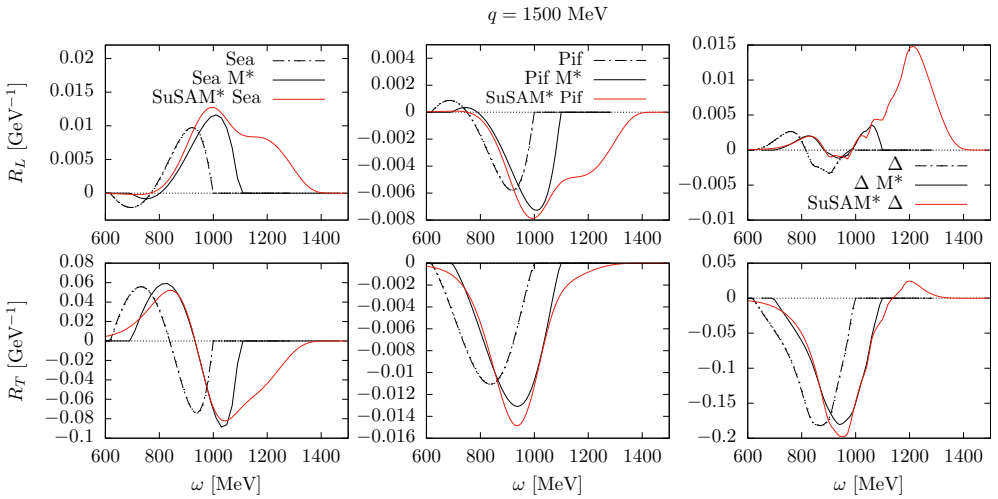

Figure 10. The same as Figure 7 for $q = 1500$ MeV/c.

First is observed that the introduction of the effective mass $M^* = 0.8$ shifts the responses to the right, towards higher energy values. The effective mass takes into account the binding of the nucleon in the nucleus, which causes the quasielastic peak to approximately coincide with the maximum of the experimental cross section. In the RFG, this is traditionally taken into account by subtracting a binding energy of approximately 20 MeV from ω to account for the average separation energy of the nucleons. In the RMF, this is automatically included by considering the effective mass of the nucleon, $M^* = 0.8$, which was adjusted for ^{12}C precisely to achieve this effect.

In the transition from the RMF to the SuSAM* model, we replace the scaling function of the RFG with the phenomenological scaling function that we have adjusted. This new scaling function extends beyond the region of $-1 < \psi^* < 1$, where the RFG scaling function is zero. As a result, we observe in Figures 7–11 that the interferences acquire a tail towards high energies, similar to the behavior of the scaling function.

The tail effect is more pronounced in the longitudinal responses because the single-nucleon longitudinal response, as shown in Figure 5, increases with ω. This amplifies the tail when multiplied by the scaling function. However, it is important to note that the contribution of the MEC to the longitudinal response is relatively small compared to the dominant transverse response. Therefore, while the tail effect is observed in the longitudinal responses, its impact on the cross section is not as significant as in the transverse channel, if not negligible.

Preprints (www.preprints.org) | NOT PEER-REVIEWED | Posted: 1 August 2023 doi:10.20944/preprints202308.0066.v1

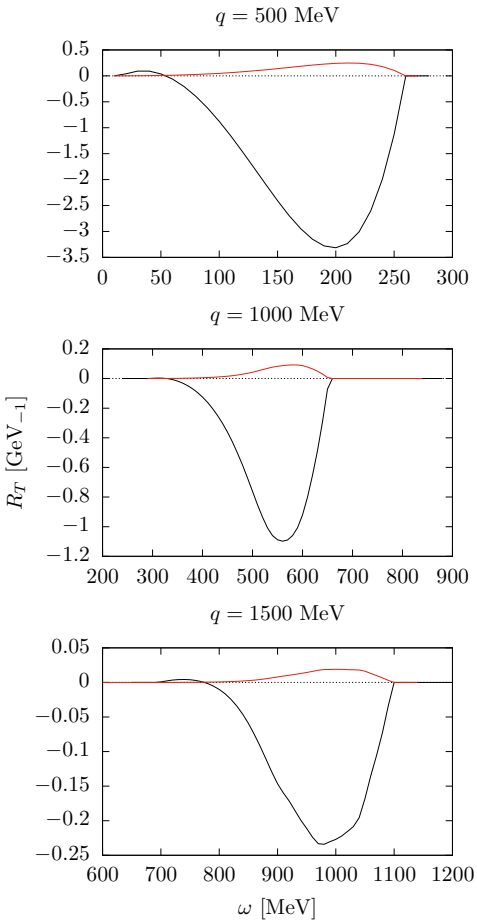

Figure 11. Comparison of OB-MEC interference in the transverse response (black lines) with the pure MEC transverse response (red lines) for several values of q in the RMF model.

In the dominant transverse response, the seagull contribution from the MEC is positive, leading to an enhancement of the response, while the pionic and Δ contributions are negative, causing a reduction in the overall response when including the MEC. This is in line with pioneering calculations by Kohno and Otsuka [46] and by Alberico *et al.* [47] in the non-relativistic Fermi gas. Also in shell model calculations, similar results have been obtained [48], showing that the MEC contributions also lead to a tail and extension of the response functions to higher values of ω, as in the SuSAM* approach. It is worth noting that the relative importance of these contributions can depend on the momentum transfer q and the energy transfer ω. For the values considered in Figures 7–11, the Δ current is found to be the dominant contribution, leading to a net negative effect from the MEC.

The observation in Figure 10 of a sign change and a small bump in the OB-Δ transverse response for high values of ω is indeed interesting. The change of sign is already observed for q=1 GeV/c in Figure 9. This connects with the findings in reference [17], where a pronounced bump and sign change were reported in a semi-relativistic shell model calculation based on the Dirac equation with a relativistic energy-dependent potential. In the present calculation the bump is observed but it is very small compared to the results of Ref, [17]. It is important to note that, in the present work, the fully relativistic SuSAM* approach is employed, which takes into account the dynamical properties of both nucleons and the Δ, as well as the scaling function. This differs from the approach in reference [17], where a static propagator for the Δ was used. To definitively clarify the difference with the present results, a fully relativistic calculation in finite nuclei, considering the dynamical properties of the Δ would be necessary.

The comparison of the OB-MEC interference with the MEC contribution alone (represented by $w_{12}^{\mu\nu}$ and $w_{2}^{\mu\nu}$, respectively in Eq, (21)) in the transverse response is shown in Figures 11 and 12. We

Preprints (www.preprints.org) | NOT PEER-REVIEWED | Posted: 1 August 2023 doi:10.20944/preprints202308.0066.v1

observe that the MEC contribution alone represents a small and almost negligible contribution to the transverse response. This justifies the previous calculations that focused only on the OB-MEC interference (e.g., the semi-analytical calculations in references [48,68] for the non-relativistic Fermi gas), as it provides an excellent approximation. This observation holds true for both the RMF model in Figure 11 and the SuSAM* model in Figure 12. It highlights the fact that the dominant contribution to the transverse response arises from the interference between the OB and MEC, while the pure MEC contribution is relatively small. It is also worth stressing that while the pure MEC contribution is, of course, positive, the interference contribution is negative.

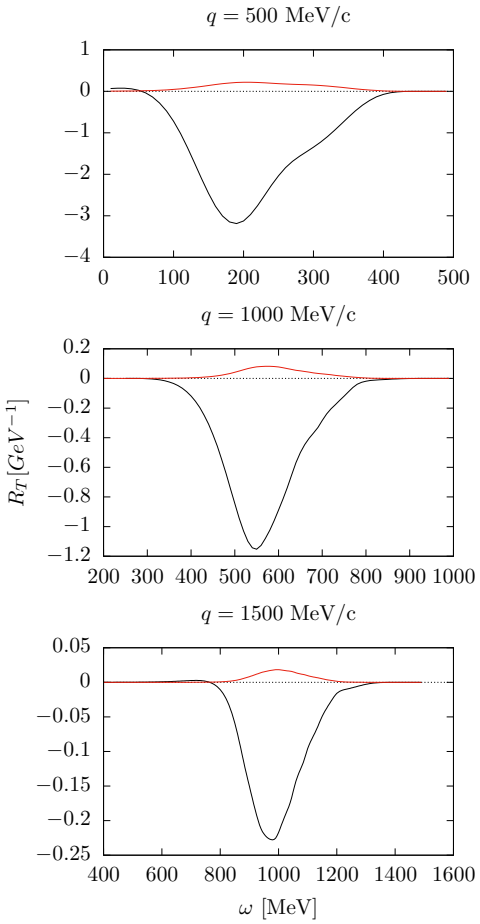

Figure 12. The same as Figure 11 in the SuSAM* model.

In Figure 13, we present the total responses of ^{12}C computed using the generalized SuSAM* model. These responses are obtained by multiplying the phenomenological scaling function by the averaged single-nucleon response and summing over protons and neutrons, as given by Eq. (36). The responses are shown for different values of q as a function of ω. In the same figure, we also show the results without including the MEC contributions, which corresponds to setting the terms $w_{12} + w_2$ associated with the two-body current (Eq. (21)) to zero.

Comparing the results with and without MEC, we observe that the impact of MEC is more significant in the transverse response compared to the longitudinal response. This is expected since the corrections due to MEC in the longitudinal response are higher-order effects in a non-relativistic expansion in powers of v/c, as known from previous studies [69]. Therefore, the MEC contributions to the longitudinal response are minimal and only start to become noticeable for q >1 GeV in the high-energy region. However, this high-energy region is dominated and overshadowed by pion emission and inelastic processes, making it difficult to isolate the 1p1h longitudinal response.

Preprints (www.preprints.org) | NOT PEER-REVIEWED | Posted: 1 August 2023 doi:10.20944/preprints202308.0066.v1

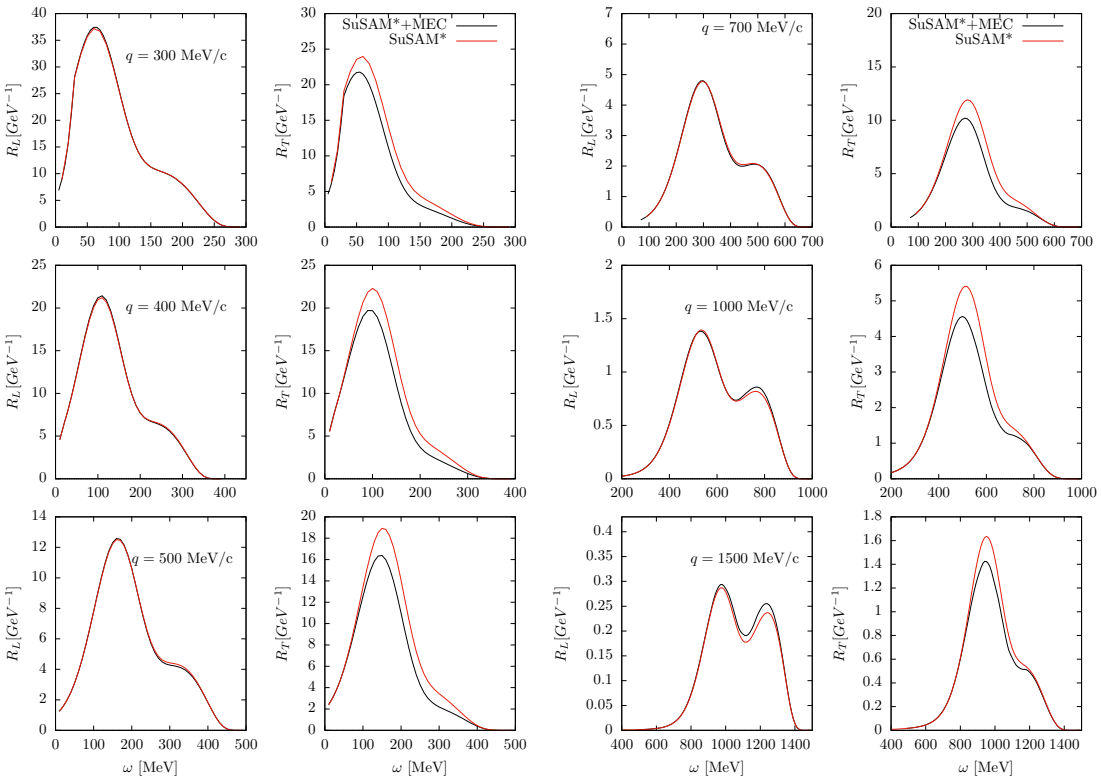

Figure 13. Response functions calculated in the generalized SuSAM* model (black curves). The red curves do not include the MEC.

The inclusion of MEC in the single-nucleon leads to a reduction of the transverse response by around 10% or even more for all studied values of q. This is consistent with previous calculations in RFG and the shell model [17,33,48,70,71]. These calculations have consistently shown that MEC in the 1p1h channel tend to decrease the transverse response compared to the contribution from the one-body current. It is important to note that this reduction in the transverse response is a direct consequence of the destructive interference between the one-body current and MEC. The contribution of MEC to the transverse response is negative because the direct two-body matrix element is zero (in symmetric nuclear matter, $N = Z$) or almost zero (in asymmetric nuclear matter, $N \neq Z$, or in finite nuclei) after summing over isospin.

The treatment of the Δ resonance in the medium is subject to various ambiguities and uncertainties. In our generalized SuSAM* model, we have assumed that the Δ resonance acquires an effective mass M^*_Δ and vector energy E^Δ_v due to its interaction with the RMF. This requires modifying the propagator according to the formalism proposed in references [25,64]. To estimate the effect of this treatment, in Figure 14 we compare the transverse response for the OB-Δ interference calculated assuming that the Δ remains unchanged in the medium, i.e., setting $M^*_\Delta = M_\Delta$ and $E^\Delta_v = 0$. The response with the free Δ without medium modifications is slightly smaller in absolute value, around 10% depending on the momentum transfer. This can be seen as an estimation of the uncertainty associated with the Δ interaction in the medium.

Preprints (www.preprints.org) | NOT PEER-REVIEWED | Posted: 1 August 2023 doi:10.20944/preprints202308.0066.v1

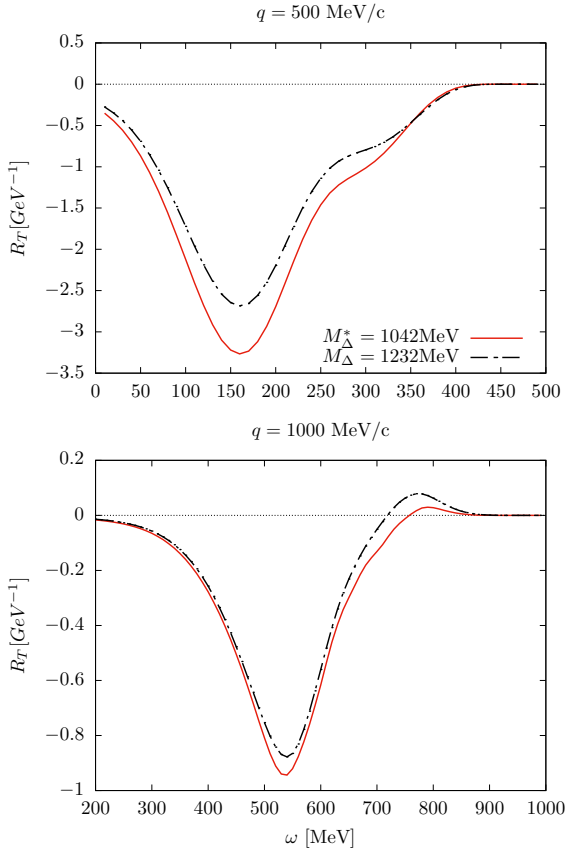

Figure 14. Comparison of the transverse interference OB-Δ computed in the generalized SuSAM* model with and without relativistic effective mass and vector energy for the Δ.

Another related issue is the modification of the Δ width in the medium, which we have not considered here assuming the free width (59). This effect can also influence the results, but it is expected to be of the same order as the observed effect in Figure 14. It is important to note that the treatment of the Δ resonance in the medium is a complex topic, and further investigations and refinements are needed to fully understand its effects and uncertainties.

In Figure 15, we compare the total transverse response calculated in the RMF model with an effective mass of $M^* = 0.8$ to the results obtained in the generalized SuSAM* approach for various momentum transfers, ranging from $q = 300$ MeV/c to $q = 1500$ MeV/c. Both calculations include the effects of MEC. One notable difference between the two approaches is the presence of a pronounced tail at high energy transfer rates in the SuSAM* results. This tail extends well beyond the upper limit of the RFG responses, reflecting the effect of the phenomenological scaling function used in the SuSAM* approach. Similar effects are found in the longitudinal response. Additionally, it is worth noting that the peak height of the transverse response in the SuSAM* approach is generally higher compared to the RMF model. Overall, the comparison in Figure 15 highlights the improvements and additional physics captured by the SuSAM* approach, by extending the scaling function of the RFG to describe the transverse response in a wider energy transfer range.

Preprints (www.preprints.org) | NOT PEER-REVIEWED | Posted: 1 August 2023 doi:10.20944/preprints202308.0066.v1

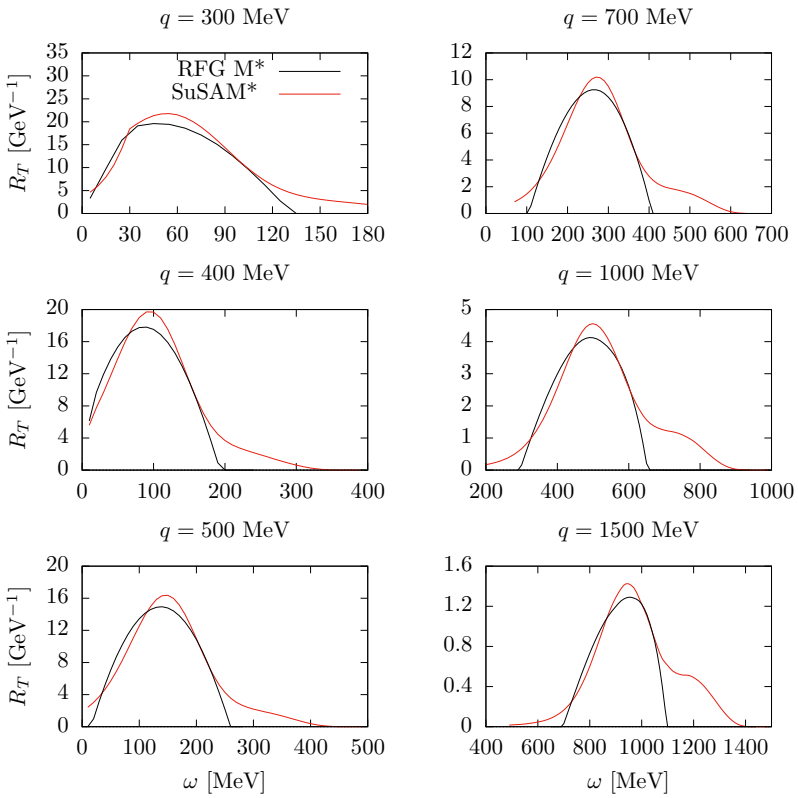

Figure 15. Total transverse responses for ^{12}C including MEC in the RMF model with $M^* = 0.8$ compared to the generalized SuSAM* model.

Finally, in Figure 16, we present the results for the (e,e') double differential cross section of ^{12}C calculated with the generalized SuSAM* model including MEC, compared to experimental data for selected kinematics. We also compare with the same model but assuming that only the single-nucleon contribution is present, i.e., setting the MEC to zero. We observe that the inclusion of MEC in this model leads to a small reduction in the cross section compared to the case without MEC. This reduction is a consequence of the decrease in the transverse response due to the presence of MEC. The generalized scaling approach, including the inclusion of MEC, provides a global description of the cross section that is comparable to other previous analyses, such as the SuSAM* model with the one-body current only, or the SuSAv2 model, which factorize different definitions of the single nucleon (without effective mass and with extrapolation of the Fermi gas single nucleon in the case of SuSAv2). All of these approaches reasonably describe the quasielastic cross section because the scaling function has been properly adjusted to reproduce the global scaling data. The generalized scaling approach, like any parametrization, is a phenomenological framework that aims to capture the essential physics of the reaction. It provides a functional form for the cross section that incorporates the known ingredients and leaves the unknowns to be determined by the scaling function. The scaling function encapsulates the effects of various dynamical and correlation effects, allowing for a global description of the data.

Preprints (www.preprints.org) | NOT PEER-REVIEWED | Posted: 1 August 2023 doi:10.20944/preprints202308.0066.v1

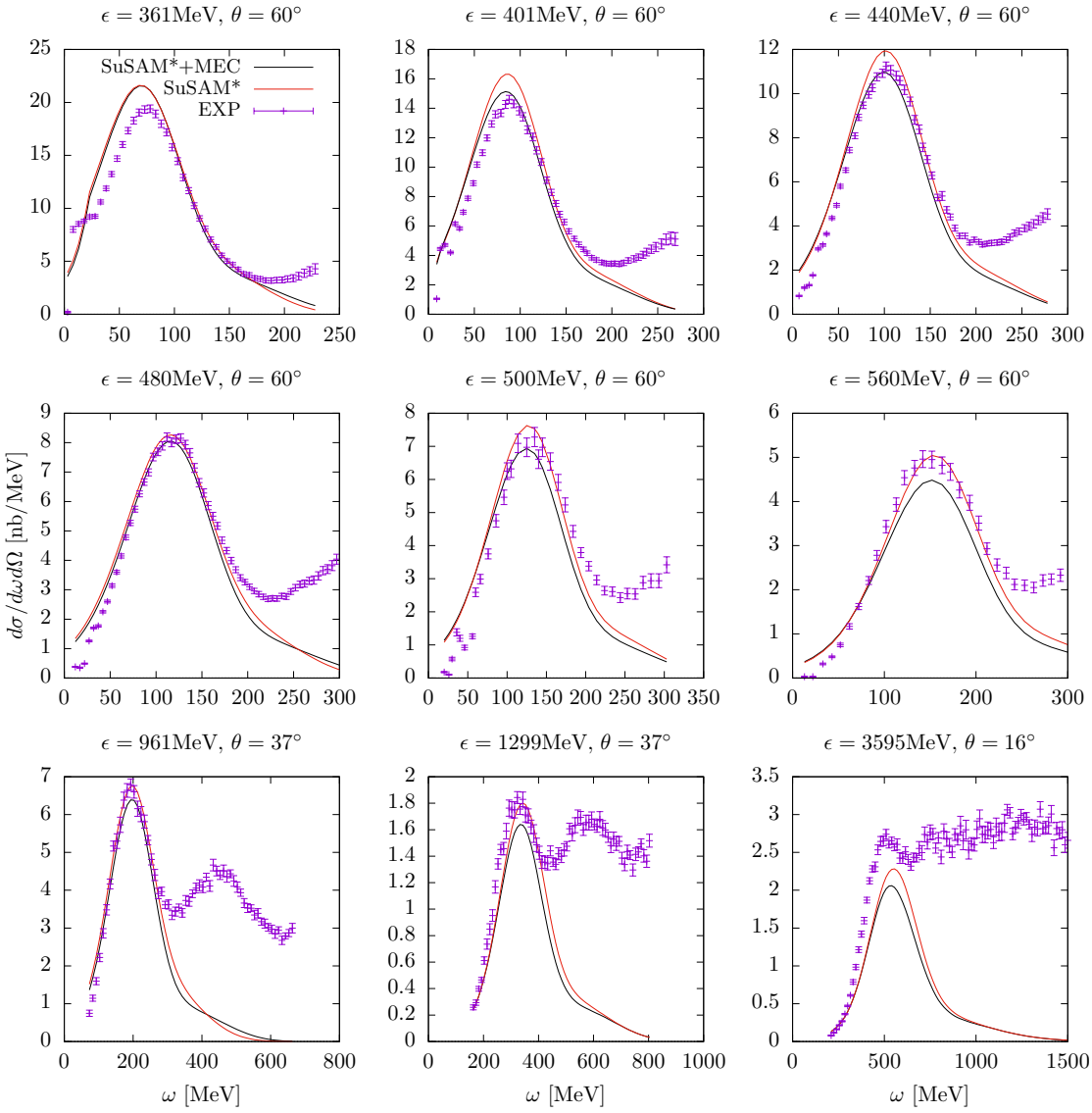

Figure 16. Cross section of ^{12}C for several kinematics computed with the generalized SuSAM* model, including MEC, compared with the same calculation without MEC. Experimental data are from Refs. [66,67].

4. Discussion and concluding remarks

From the results seen in the previous section we have observed that, in all the models considered, the transverse response decreases when including meson exchange currents in the 1p1h channel. This result is consistent with previous independent calculations performed in the relativistic and non-relativistic Fermi gas models as well as in the non-relativistic and semi-relativistic shell models. The result is a consequence of the fact that the main contribution arises from the interference of the OB and Δ currents, in particular through the exchange diagram, carrying a minus sign. The contribution from the direct part of the MEC matrix element is zero in the Fermi gas, and this is the reason for the negative contribution.

It is worth mentioning the existence of some calculations that disagree with this result and suggest a different effect of MEC on the transverse response. We would like to comment in particular on two notable model calculations: the Green Function Monte Carlo (GFMC) model from reference [72] and the Correlated Basis Function (CBF) calculation by Fabrocini [70], both including meson exchange currents in the 1p1h sector. In both approaches, the effect of MEC is positive in the quasielastic peak and quite significant, around 20%, in the transverse response. This substantial effect is attributed to

 doi:10.20944/preprints202308.0066.v1

the simultaneous effect of tensor correlations in the wave function and MEC. In fact, in Fabrocini's calculation, the origin of this effect was found to be the tensor-isospin correlation contribution in the direct matrix element of the Δ current, which is non-zero when summing over isospin for correlated wave functions. This effect can also be understood in terms of presence of short-range correlations in the nuclear wave function. The direct matrix element of MEC, when a proton is emitted, involves the interaction of the proton with protons as well as with neutrons, i.e., the MEC matrix element involves PN and PP pairs. The high-momentum component of these pairs is significantly different because PN pairs contain the $^3S_1$ and $^3D_1$ deuteron-like waves, while PP pairs do not. Therefore, when summing over isospin, there is no cancellation between PP and PN pairs in the high-momentum part of the wave function, resulting in a non-zero direct matrix element. This is in agreement with the conclusion of Fabrocini, as the tensor-isospin term precisely generates this significant difference between PP and PN pairs. An alternative way to investigate this hypothesis would be to perform calculations in the independent particle model by solving the Bethe-Goldstone equation [73] for PP and PN pairs and using a correlation current similar to the one proposed in [74]. Such calculations could provide further insights into the effect of short-range correlations on the MEC contributions to the transverse response.

On the other hand the results of Fabrocini reproduce the well-known effect that MEC has a negative impact on the transverse response when the correlations functions are set to zero, consistent with the results from uncorrelated models. Since in the present work we started with an uncorrelated model, the relativistic mean field, the effects of correlations in the transverse current are expected to be included phenomenologically in the scaling function. This and other mechanisms, such as final state interactions, contribute to the violation of scaling observed in the data.

To summarize, this work presents a generalized scaling analysis of the (e,e') cross section of ^{12}C, including the MEC consistently in the formalism. To achieve this, we have introduced a new definition of the single nucleon tensor in the factorization of the model. The average per particle of the hadronic tensor for 1p1h emission has been defined by considering the sum of the one-body and two-body currents, without modifying the definition of the scaling function, which remains the same as in the one-body current case in the Fermi gas. This averaging definition has been extended beyond the scaling region $-1 < \psi^* < 1$ of the Fermi gas by slightly modifying the momentum distribution with a smeared Fermi distribution that allows the evaluation of MEC for any value of the scaling variable.

By incorporating the MEC and using the phenomenological scaling function, we have calculated the 1p1h response functions in the RFG, RMF, and SuSAM* models. The results show the impact of the MEC on the response functions, particularly in the transverse sector. The MEC reduce the transverse response while the longitudinal response is found to be hardly affected by the MEC. Furthermore, the analysis of the OB-MEC interference and the comparison between the SuSAM* and RFG models highlight the role of the effective mass and the Δ resonance in the response functions.

Overall, the generalized scaling analysis with the inclusion of MEC provides a consistent framework for studying quasielastic electron scattering in nuclei accounting for relativistic dynamical effects through the effective mass. The approach adopted in this work differs from other scaling analyses, such as the original SuSAM* model, in the definition of the single-nucleon dividing factor, which now incorporated the effect of MEC in the 1p1h channel. However, the ultimate results are compatible between different models because the improvement in scaling symmetry is not significant when modifying the single nucleon in this manner. This means that both formalisms will describe the experimental cross section data similarly, as they have been adjusted accordingly. The difference between various approaches lies in how the scaling function is adapted and rectified based on the chosen prefactor of the single nucleon. The equivalence between these models and others, such as SuSAv2, indicates the flexibility of the scaling approach to adapt to the circumstances of the emphasized model. Scaling is only an approximate symmetry of quasielastic data, and the degree of violation of this symmetry should be attributed to all effects that break the factorization of the cross section in a many-body system with complex interactions and correlations between particles.

In conclusion, this work presents the first comprehensive study of quasielastic electron scattering in nuclei that includes the 1p1h meson exchange currents (MEC) consistently in a generalized scaling approach, extending previous work where this contribution was evaluated in the relativistic Fermi gas (RFG) framework. Looking ahead, this work opens the door to future developments and applications, including the extension of the model to study neutrino-nucleus scattering.

Author Contributions: All authors contributed to conceptualisation, methodology, software, validation, investigation, and writing. All authors have read and agreed to the published version of the manuscript.

Funding: Work supported by: Grant PID2020-114767GB-I00 funded by MCIN/AEI /10.13039 /501100011033; FEDER/Junta de Andalucia-Consejeria de Transformacion Economica, Industria, Conocimiento y Universidades/A-FQM-390-UGR20; Junta de Andalucia (Grant No. FQM-225); INFN under Project NUCSYS; and University of Turin under Project BARM-RILO-23-01.

Data Availability Statement: Cross section datasets analyzed available at Refs. [66,67].

Conflicts of Interest: The authors declare no conflict of interest.

Abbreviations

The following abbreviations are used in this manuscript:

OB	One-body
MEC	Meson-exchange currents
RFG	Relativistic Fermi Gas
RMF	Relativistic mean field
SuSA	Superscaling analysis
SuSAM*	Superscaling analysis with relativistic effective mass

References

1. Y. Fukuda *et al.* [Super-Kamiokande], Phys. Rev. Lett. **81** (1998) 1562
2. P. Adamson *et al.* [NOvA], Phys. Rev. Lett. **116** (2016) 151806
3. A. A. Aguilar-Arevalo et al. (MiniBooNE Collaboration), Phys. Rev. D 81, 092005 (2010).
4. K. Abe, J. Amey, C. Andreopoulos, L. Anthony, M. Antonova, S. Aoki, A. Ariga, Y. Ashida, Y. Azuma, S. Ban, and et al., Physical Review D 98 (2018)
5. R. Acciarri, C. Adams, J. Asaadi, B. Baller, T. Bolton, C. Bromberg, F. Cavanna, E. Church, D. Edmunds, A. Ereditato, and et al., Physical Review D 89 (2014),
6. M. A. Acero et al. (NOvA), Phys. Rev. Lett. 123, 151803 (2019),
7. L. Alvarez-Ruso, Y. Hayato, J. Nieves, New J. Phys. 16 (2014) 075015.
8. U. Mosel, Ann. Rev. Nuc. Part. Sci. 66 (2016), 171.
9. T. Katori and M. Martini, J. Phys. G **45** (2018) no.1, 013001.
10. A. M. Ankowski, C. Mariani, J. Phys. G44 (2017) 054001.
11. O. Benhar, P. Huber, C. Mariani, D. Meloni, Phys. Rep. 700 (2017) 1.
12. L. Alvarez-Ruso et al. (NuSTEC), Prog. Part. Nucl. Phys. 100 (2018) 1
13. J. E. Amaro, M. B. Barbaro, J. A. Caballero, T. W. Donnelly, A. Molinari and I. Sick, Phys. Rev. C **71**, 015501 (2005).
14. J. E. Amaro, M. B. Barbaro, J. A. Caballero, R. González-Jiménez, G. D. Megias and I. Ruiz Simo, J. Phys. G **47** (2020) no.12, 124001
15. J. E. Amaro, M. B. Barbaro, J. A. Caballero, T. W. Donnelly, R. Gonzalez-Jimenez, G. D. Megias and I. R. Simo, Eur. Phys. J. ST **230** (2021) 4321
16. A. M. Ankowski, A. Ashkenazi, S. Bacca, J. L. Barrow, M. Betancourt, A. Bodek, M. E. Christy, L. D. S. Dytman, A. Friedland and O. Hen, *et al.*
17. J. E. Amaro, M. B. Barbaro, J. A. Caballero, T. W. Donnelly, C. Maieron and J. M. Udias, Phys. Rev. C **81**, 014606 (2010)
18. G. D. Megias, J. E. Amaro, M. B. Barbaro, J. A. Caballero and T. W. Donnelly, Phys. Rev. D **94**, 013012 (2016)
19. J. E. Amaro, E. Ruiz Arriola and I. Ruiz Simo, Phys. Rev. D **95**, no.7, 076009 (2017)
20. T. W. Donnelly, S. Jeschonnek and J. W. Van Orden, Annals Phys. **448**, 169174 (2023)

21. T. W. Donnelly, Universe **9** (2023), 196
22. R. Rosenfelder, Ann. Phys. (N.Y.) 128, 188 (1980).
23. B.D. Serot, and J.D. Walecka, Adv. Nucl. Phys. 16 (1986) 1.
24. D Drechselt and M M Giannini, Rep. Prog. Phys. 52 (1989) 1083.
25. K. Wehrberger, Phys. Rep. 225 (1993) 273.
26. M.B. Barbaro, R. Cenni, A. De Pace, T.W. Donnelly, A. Molinari, Nucl. Phys. A 643 (1998) 137.
27. C. Giusti, A. Meucci, M. V. Ivanov and J. M. Udias, Nucl. Theor. **34**, 34-44 (2015)
28. V. Pandey, N. Jachowicz, T. Van Cuyck, J. Ryckebusch and M. Martini, Phys. Rev. C **92**, no.2, 024606 (2015)
29. M. Martini, N. Jachowicz, M. Ericson, V. Pandey, T. Van Cuyck and N. Van Dessel, Phys. Rev. C **94**, no.1, 015501 (2016)
30. R. González-Jiménez, A. Nikolakopoulos, N. Jachowicz and J. M. Udías, Phys. Rev. C **100**, no.4, 045501 (2019)
31. A. Lovato, J. Carlson, S. Gandolfi, N. Rocco, and R. Schiavilla, Phys. Rev. X 10, 031068 (2020), arXiv:2003.07710 [nucl-th].
32. J. E. Amaro, M. B. Barbaro, J. A. Caballero, T. W. Donnelly and A. Molinari, Phys. Rept. **368**, 317-407 (2002)
33. J. E. Amaro, M. B. Barbaro, J. A. Caballero, T. W. Donnelly and A. Molinari, Nucl. Phys. A **723** (2003), 181-204
34. J. E. Amaro, M. B. Barbaro, J. A. Caballero, T. W. Donnelly, C. Maieron and J. M. Udias, Phys. Rev. C **81** (2010), 014606
35. W. M. Alberico, M. Ericson and A. Molinari, Annals Phys. **154**, 356 (1984)
36. J. W. Van Orden and T. W. Donnelly, Annals Phys. **131** (1981), 451-493
37. M. J. Dekker, P. J. Brussaard and J. A. Tjon, Phys. Rev. C **49**, 2650-2670 (1994)
38. M. Martini, M. Ericson, G. Chanfray and J. Marteau, Phys. Rev. C **81**, 045502 (2010)
39. O. Lalakulich, K. Gallmeister and U. Mosel, Phys. Rev. C **86**, no.1, 014614 (2012) [erratum: Phys. Rev. C **90**, no.2, 029902 (2014)]
40. J. Nieves, I. Ruiz Simo and M. J. Vicente Vacas, Phys. Lett. B **721**, 90-93 (2013)
41. T. Van Cuyck, N. Jachowicz, R. González-Jiménez, J. Ryckebusch and N. Van Dessel, Phys. Rev. C **95**, no.5, 054611 (2017)
42. A. De Pace, M. Nardi, W. M. Alberico, T. W. Donnelly and A. Molinari, Nucl. Phys. A **726**, 303-326 (2003)
43. I. Ruiz Simo, J. E. Amaro, M. B. Barbaro, A. De Pace, J. A. Caballero and T. W. Donnelly, J. Phys. G **44**, no.6, 065105 (2017)
44. V. L. Martinez-Consentino, I. R. Simo and J. E. Amaro, Phys. Rev. C **104**, no.2, 025501 (2021)
45. V. L. Martinez-Consentino, J. E. Amaro and I. Ruiz Simo, Phys. Rev. D **104**, no.11, 113006 (2021)
46. M. Kohno and N. Ohtsuka, Phys. Lett. B **98** (1981), 335-339 doi:10.1016/0370-2693(81)90919-9
47. W. M. Alberico, T. W. Donnelly and A. Molinari, Nucl. Phys. A **512**, 541-590 (1990)
48. J. E. Amaro, A. M. Lallena and G. Co, Nucl. Phys. A **578** (1994), 365-396
49. A. Meucci, C. Giusti and F. D. Pacati, Phys. Rev. C **66**, 034610 (2002)
50. V. L. Martinez-Consentino, I. Ruiz Simo, J. E. Amaro and E. Ruiz Arriola, Phys. Rev. C **96**, no. 6, 064612 (2017).
51. J. E. Amaro, V. L. Martinez-Consentino, E. Ruiz Arriola and I. Ruiz Simo, Phys. Rev. C **98** (2018) no.2, 024627
52. T. W. Donnelly and I. Sick, Phys. Rev. C **60**, 065502 (1999)
53. R. Gonzaléz-Jiménez, G. D. Megias, M. B. Barbaro, J. A. Caballero and T. W. Donnelly, Phys. Rev. C **90** (2014) no.3, 035501
54. G. D. Megias, J. E. Amaro, M. B. Barbaro, J. A. Caballero, T. W. Donnelly and I. Ruiz Simo, Phys. Rev. D **94**, no.9, 093004 (2016)
55. I. Ruiz Simo, V. L. Martinez-Consentino, J. E. Amaro and E. Ruiz Arriola, Phys. Rev. D **97**, 116006 (2018).
56. J. E. Amaro, E. Ruiz Arriola and I. Ruiz Simo, Phys. Rev. C **92**, no.5, 054607 (2015) [erratum: Phys. Rev. C **100**, no.1, 019904 (2019)]
57. P.R. Casale, J.E. Amaro, V.L. Martinez-Consentino, I. Ruiz Simo Universe **9** (2023) 158.
58. Pascalutsa and O. Scholten, Nucl. Phys. A 591 658 (1995).
59. B. Sommer, Nucl. Phys. A **308** (1978)
60. T.O. Ericson and W. Weise, Pions and Nuclei (Oxford University Press, New York 1988).
61. C. H. Llewellyn Smith, Phys. Rept. **3**, 261-379 (1972)
62. E. Hernandez, J. Nieves and M. Valverde, Phys. Rev. D **76**, 033005 (2007)

63. J.J. Quiros, C. Barbero, D.E. Jaramillo, A. Mariano, J. Phys. G: Nucl. Part. Phys. **44** (2017) 045112.
64. H. C. Kim, S. Schramm and C. J. Horowitz, Phys. Rev. C **53**, 2468-2473 (1996)
65. J.Hockert, D.O. Riska, M. Gari, A. Huffman, Nucl. Phys. **A217** (1973) 14.
66. O. Benhar, D. Day and I. Sick, arXiv:nucl-ex/0603032.
67. O. Benhar, D. Day, and I. Sick, http://faculty.virginia.edu/qes-archive/
68. J. E. Amaro, A. M. Lallena and G. Co, Int. Jou. Mod. Phys **E 3** (1994), 735.
69. D.O. Riska, Phys. Rep. 181 (1989) 207.
70. Adelchi Fabrocini, Phys. Rev. C **55** (1997) 338.
71. J. E. Amaro, M. B. Barbaro, J. A. Caballero and F. Kazemi Tabatabaei, Phys. Rev. C **68**, 014604 (2003).
72. A. Lovato, S. Gandolfi, J. Carlson, S. C. Pieper and R. Schiavilla, Phys. Rev. Lett. **117**, no.8, 082501 (2016)
73. P. R. Casale, J. E. Amaro, E. Ruiz Arriola and I. Ruiz Simo, [arXiv:2304.00296 [nucl-th]].
74. V.L. Martinez-Consentino, J.E. Amaro, P.R. Casale, I Ruiz Simo. Phys. Rev. D (2023) in press, [arXiv:2210.09982 [nucl-th]].